Water mass transformation in the Greenland Sea during the 1990s

J. Karstensen,[1,2] P. Schlosser,[3,4] D. W. R. Wallace,[1] J. L. Bullister,[5] and J. Blindheim[6]

Received 28 May 2004; revised 9 February 2005; accepted 2 May 2005; published 27 July 2005.

[1] Time series of hydrographic and transient tracer measurements were used to study the variability of Greenland Sea water mass transformation between 1991 and 2000. Increases in tracer inventories indicate active renewal of Greenland Sea Intermediate Water (GSIW) at a rate of 0.1 to 0.2 Sv (1 Sv = 1×10^6 m^3 s^{-1}) (10-year average). A temperature maximum (T_{max}) was established at the base of the upper layer (500 m) as a consequence of anomalously strong freshwater input into the near-surface layer at the beginning of the 1990s. T_{max} rapidly descended to 1500 m by 1995 followed by a much slower rate of descent. GSIW became warmer and less saline compared to the 1980s. During the deepening phase of T_{max}, atmospheric data revealed above-average wind stress curl and oceanic heat loss. In addition, high Arctic Ocean sea-ice export and lack of local sea-ice formation have been documented for that period. A combination of all these factors may have evoked the renewal of GSIW with anomalously freshwater from the upper layers. The T_{max} layer established a stability maximum that inhibits vertical exchange between intermediate and deeper waters. Temperature and salinity of deep waters continued to increase at rates of 0.01°C yr^{-1} and 0.001 yr^{-1}, respectively. However, since 1993, decrease in and homogenization of deep water transient tracer concentrations indicate that renewal occurred predominantly by addition of Arctic Ocean waters. In 2000 the water column (500 m to 3400 m) required an additional 60 W m^{-2} (110 W m^{-2}) over the annual mean heat loss to restore its heat content to 1989 (1971) values.

Citation: Karstensen, J., P. Schlosser, D. W. R. Wallace, J. L. Bullister, and J. Blindheim (2005), Water mass transformation in the Greenland Sea during the 1990s, *J. Geophys. Res.*, *110*, C07022, doi:10.1029/2004JC002510.

1. Introduction

[2] The Arctic Mediterranean comprises the Arctic Ocean, as well as the Greenland, Norwegian, and Iceland seas (GIN seas) including the deep basins and rather wide shallow areas such as the Barents Sea [*Aagaard et al.*, 1985]. This region is linked to the North Atlantic through the Greenland-Iceland-Scotland overflows and is an important water mass transformation area in the world ocean. The upper layer circulation in the gyres of the GIN seas is cyclonic. Within the Arctic Mediterranean, warm and saline Atlantic water masses are successively transformed into colder and fresher waters which leaves the region via the overflows and provides a major component of the North Atlantic Deep Water (NADW). Each of the deep basins in the GIN seas is characterized by a cyclonic gyre linked to the topography [*Poulain et al.*, 1996; *Jakobsen et al.*, 2003].

[3] At present, most of the overflowing waters are generated by rather shallow convection and subduction in the Norwegian, Iceland, and Greenland seas and through gradual transformation of Atlantic Water [*Swift et al.*, 1980; *Mauritzen*, 1996; *Hansen and Osterhus*, 2000]. However, deep water renewal in the region is also important as it maintains the interior overturning of the Arctic Mediterranean. A key region for direct deep water renewal is the central Greenland Sea. Here the water column is characterized by a weak stratification and has the densest outcrop in winter. Although never directly observed, extreme properties observed in the bottom waters indicate that intermittent renewal of deep and bottom waters takes place in the center of the Greenland Sea gyre [e.g., *Alekseev et al.*, 1994; *Meincke et al.*, 1997; *Bönisch et al.*, 1997].

[4] Transformation of surface water in the GIN seas is controlled by air-sea-ice interaction including surface cooling, brine release, and meltwater addition. These processes are highly variable in time and space and may correlate with large-scale atmospheric modes such as the North Atlantic Oscillation (NAO) or the Arctic

[1]Leibniz Institut für Meereswissenschaften an der Universität Kiel (IFM-GEOMAR), Kiel, Germany.
[2]Formerly at Lamont-Doherty Earth Observatory of Columbia University, Palisades, New York, USA.
[3]Lamont-Doherty Earth Observatory of Columbia University, Palisades, New York, USA.
[4]Also at Department of Earth and Environmental Sciences/Department of Earth and Environmental Engineering, Columbia University, New York, New York, USA.
[5]NOAA/Pacific Marine Environmental Laboratory, Seattle, Washington, USA.
[6]Havforskningsinstituttet, Bergen, Norway.

0148-0227/05/2004JC002510$09.00

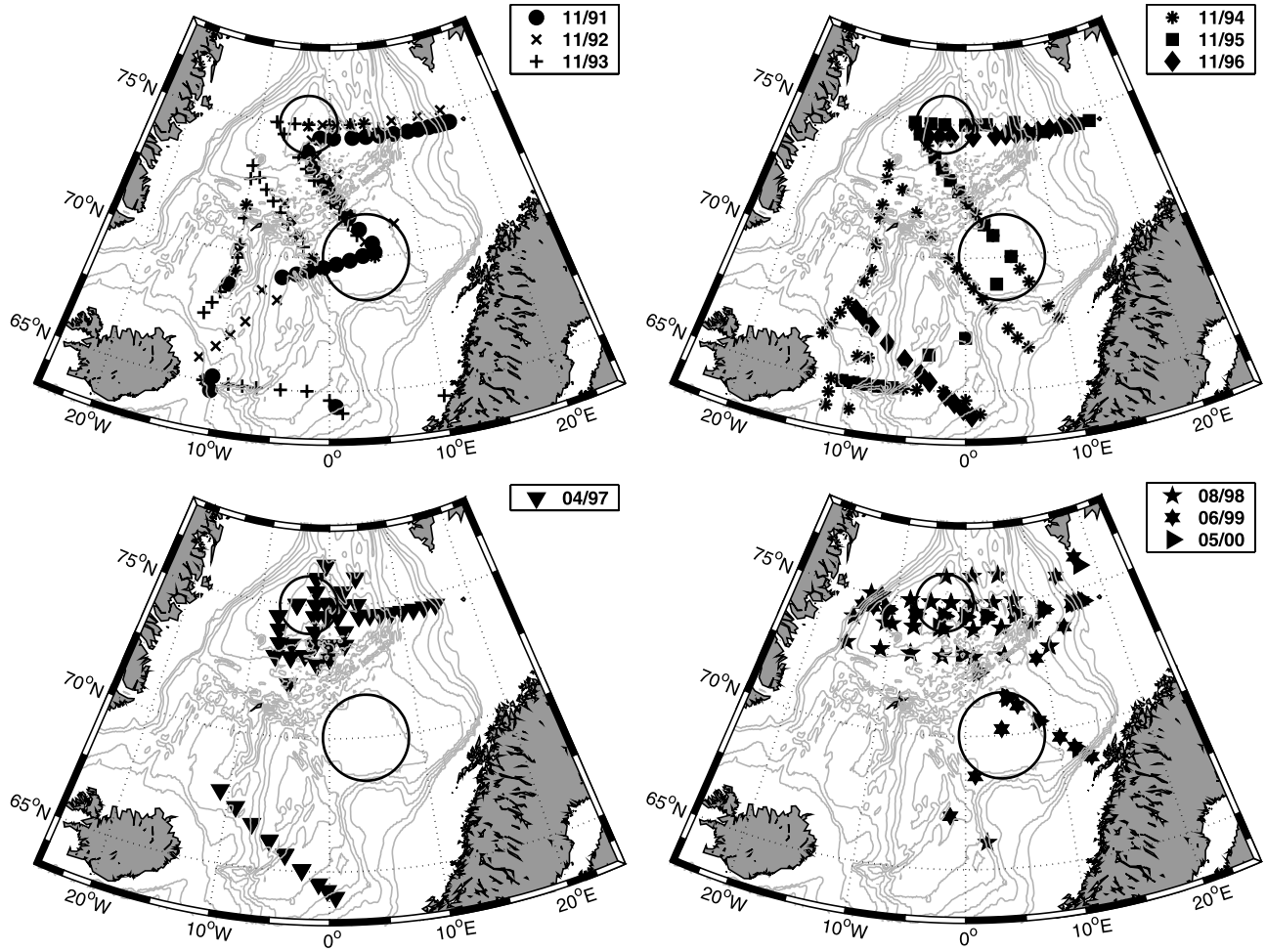

Figure 1. Station maps of RV *Johan Hjort* cruises in the Norwegian and Greenland Sea. Circled regions indicate the locations of the central gyres. Topography contours are draw in 500-m steps from 500 m to 3500 m.

Oscillation (AO). Model studies and paleo data have shown that changes in the freshwater flux (including effects of sea-ice formation and melting) in the northern North Atlantic and GIN seas may inhibit convection and in turn have major impact on the patterns and strength of the global thermohaline circulation [e.g., *Broecker et al.*, 1990; *Rahmstorf*, 1994; *Vellinga and Wood*, 2002].

[5] Changes in the thermohaline structure of the upper and intermediate waters in the GIN seas can affect transport rates and properties of the overflow water and thus the water mass composition and circulation throughout the Atlantic [*Bacon*, 1997; *Hansen and Osterhus*, 2000]. Changes in the formation of GIN seas deep and bottom waters have less direct effects outside the Arctic Mediterranean because these deep waters are formed at lower rates and do not contribute directly to the overflows. However, formation of the deep and bottom water masses can act as important sinks for heat and salt and help maintain the overall pressure (density) gradient between the open North Atlantic and the GIN seas, thus contributing to the driving force for the overflow [*Bacon*, 1997; *Hansen and Osterhus*, 2000]. Model studies and observations [*Hansen et al.*, 2001] indicate that the formation of less dense deep water would reduce this density contrast and weaken the thermohaline circulation in the GIN seas.

[6] As part of the Atlantic Climate Change Program (ACCP) and CLIVAR (Climate Variability and Prediction) Atlantic activities, transient tracer measurements were performed in the GIN seas on an annual basis between 1991 and 2000 in the framework of repeat hydrographic cruises by the Institute of Marine Research (IMR) in Bergen, Norway. Although the station spacing varied somewhat from year to year (Figure 1), the cruises followed quasi-standard lines. One of those lines, at about 75°N, crossed the central Greenland Sea each year and, in conjunction with data from earlier cruises, provides one of the longest time series of transient tracer measurements [*Bönisch et al.*, 1997]. The purpose of this study is to use an annually resolved transient tracer time series in combination with hydrographic data to identify and explain temporal variability in water mass transformation/renewal in the Greenland Sea gyre. We build upon the prior study of *Bönisch et al.* [1997] that focused almost exclusively on the renewal of the deep and bottom waters. Our study pays particular attention to intermediate

Table 1. Transient Tracer Data Set Inventory

Cruise Date, mm/yyyy	CCl_4	CFC-11	CFC-12	CFC-113	^3H	δ^3He	^4He
11/1991	310	338	0	0	85	92	93
11/1992	322	339	335	299	134	169	171
11/1993	0	560	560	551	100	104	114
11/1994	915	919	918	854	116	136	137
11/1995	436	436	434	423	125	127	130
11/1996	291	290	291	291	72	60	68
05/1997	786	792	782	782	28	26	30
08/1998	498	495	463	449	56	46	63
06/1999	486	486	486	486	84	72	110
06/2000	384	546	546	546	21	13	70

water formation and its connection to forcing at the air-sea-ice interface.

2. GIN Seas

[7] The Greenland Sea (GS) gyre is part of the GIN seas and covers an area of approximately 9×10^5 km^2 [*Jakobsson*, 2002] with depths reaching about 3600 m. The upper layer circulation is cyclonic and is bound by two frontal zones: the Arctic Front in the east, associated with the West Spitzbergen Current, and the Polar Front in the west, associated with the East Greenland Current (EGC). The Jan-Mayen Current in the south closes the cyclonic circulation. The wind-driven cyclonic circulation over the Greenland Sea favors a weak stratification in the gyre center and allows comparably deep convection to occur in winter. The gyre exchanges laterally with the warm, saline Atlantic inflow on its eastern side, as well as the cold, fresh Arctic outflow to the west. However, the Atlantic inflow can even be identified in the west as a subsurface maximum in temperature and salinity [e.g., *Rudels et al.*, 1989; *Aagaard et al.*, 1991]. Hence lateral mixing and penetration of water from the gyre rim toward the center of the Greenland Sea increases temperature while local winter cooling decreases temperature. The near-surface salinity is controlled through a balance between lateral intrusion of saline Atlantic Water and the low-salinity water from the East Greenland current (EGC). Both sources are variable in time and play an important role in the seasonal stratification and hence preconditioning for convection in the central Greenland Sea gyre. The deep and bottom waters of the Greenland Sea gyre are the coldest and densest in the entire Arctic Mediterranean. One source water is derived locally from the upper layers of the gyre and added to the deep and bottom waters through intermittent deep convective events thereby forming their densest mode [*Aagaard et al.*, 1985; *Schlosser et al.*, 1991; *Rudels*, 1990; *Meincke et al.*, 1997; *Bönisch et al.*, 1997]. However, lateral mixing of water of Arctic Ocean origin, as well as vertical mixing [*Aagaard et al.*, 1991; *McDougall*, 1983; *Meincke et al.*, 1997; *Visbeck and Rhein*, 2000] also modify the properties of deep and bottom water.

[8] The Norwegian Sea covers an area of about 13×10^5 km^2 [*Jakobsson*, 2002] and is located southeast of the Greenland Sea (centered at about 71°N and 5°E). With maximum depths of about 3700 m it is separated from the Greenland Sea by the Mohns Ridge and further south by the Jan-Mayen Ridge. The Norwegian Sea has two deep basins: the Lofoten Basin in the north and the Norwegian Basin in the south. Both basins exhibit a weak cyclonic circulation [*Poulain et al.*, 1996; *Jakobsen et al.*, 2003]. There is no observational evidence for significant deep convection in the Norwegian Sea. However, significant water mass transformation of the inflowing Atlantic Water takes place in the upper layer of the Norwegian Sea through intense air-sea interaction. The transformed waters supply most of the Faroe-Shetland overflow [*Mauritzen*, 1996; *Hansen and Osterhus*, 2000]. The deep waters of the Norwegian Sea enter from the north and are a mixture of Greenland Sea Deep Water and deep water of the Arctic Ocean (AODW) that mix outside the Norwegian Sea near Fram Strait [*Smethie et al.*, 1986; *Swift and Koltermann*, 1988; *Heinze et al.*, 1990; *Rudels et al.*, 2000].

[9] The Iceland Sea gyre (centered at about 68°N and 10°W) comprises an area of 4×10^5 km^2 [*Jakobsson*, 2002] with a maximum depth of about 2000 m. It is roughly defined as the water body located to the west of Jan Mayen Ridge at about 8°W, between the Norwegian Sea to the east, the Greenland Sea to the north, the Denmark Strait to the west, and the North Atlantic Ocean to the south. The Iceland Sea is an important region for renewal of intermediate depth waters within the GIN seas [e.g., *Swift and Aagaard*, 1981]. The Iceland gyre interacts with the Arctic outflow in the East Greenland Current, with inflowing Atlantic Water and with a subsurface supply of water of Greenland Sea origin. Waters leaving the GIN seas via the Denmark Strait overflow acquire their final characteristics through local water mass formation in the Iceland Sea [e.g., *Swift and Aagaard*, 1981; *Hansen and Osterhus*, 2000; *Jonsson and Valdimarsson*, 2004].

3. Data Set

[10] The data set used in this study consists of transient tracer (CFC-11, CFC-12, CFC-113, CCl_4, ^3He, and tritium) and hydrographic data that were collected during annual cruises of the Norwegian Research Vessel *Johan Hjort* to the GIN seas region between 1991 and 2000.

[11] Approximately 5000 CFC and CCl_4 samples, as well as 800 $^3H/^4He$ samples, were collected within the region between 62°N to 78°N, and 20°W to 30°E (see Figure 1 and Table 1) with a 12-position Rosette/Carousel sampler using 10-L Niskin bottles. The CFC measurement program for the period between 1991 and 1995 was headed by the Brookhaven National Laboratory (BNL) and those for the period between 1996 and 2000 by NOAA's Pacific Marine Environmental Laboratory (PMEL). Air samples were routinely collected along the cruise tracks and analyzed for CFCs and CCl_4. Both air and water samples were analyzed at sea [*Bullister and Weiss*, 1988] and calibrated using gas-phase standards the concentrations of which were traceable to the SIO-1998 calibration scale [*Prinn et al.*, 2000; *Walker et al.*, 2000]. In 1991 and 1992, no gas-phase standards for CCl_4 and CFC-113 were available at sea, and the initial calibration of these compounds in water samples was relative to analysis of air performed during the cruises. Since only small gradients were expected in the concentrations of these compounds in the atmosphere over the North Atlantic, final calibration of the water samples was based on the assumption that the CCl_4 and CFC-113 concentrations in air samples measured during the cruises were the same as the

3-month average ALE-GAGE CCl_4 and CFC-113 atmospheric values measured at Adrigole, Ireland [*Prinn et al.*, 2000], during the time period of each cruise. Absolute accuracy of the data relative to the SIO-1998 scale varied slightly from one compound to another and from cruise to cruise, depending on the standard and calibration methods used. The precision of the measurements, estimated from the standard deviation of replicate analysis, for data collected after 1994 (before 1995) is about 1% (2%) or 0.01 pmol kg^{-1} (0.01 pmol kg^{-1}), whichever is greater, for CFC-12 and CFC-11, and 5% (5%) for CFC-113 and for CCl_4. Systematic sampling and calibration errors are estimated to be of the same order. Overall, we consider that CFC-11 and CFC-12 have the best data quality for the entire set of our CFC/CCl_4 time series.

[12] The tritium and helium isotope measurements were performed at the Lamont-Doherty Earth Observatory (L-DEO) Noble Gas Laboratory (NGL). For details of the analytical procedure and measurement precision, see *Ludin et al.* [1998]. The ^{3}He data are reported in the δ notation, i.e., $\delta^3He = ((R_s/R_a) - 1) \times 100\%$ where R_s is the $^3He/^4He$ ratio of the sample, and R_a is that of the standard (air). ^{4}He concentrations are reported in cm^3 STP g^{-1}, and tritium (^{3}H) concentrations in Tritium Units (TU; one TU means a ^{3}H to H ratio of 10^{-18}). The precision of δ^3He is ±0.2%, and that of the ^{4}He concentrations is ±0.5%. The typical precision of the tritium data is ±2% or ±0.05 TU, whichever error is larger.

[13] CTD data were obtained by using a Neil Brown Mark IIIb (1991 and 1992), and a Seabird 911+ equipped with dual temperature and conductivity sensors (1993 to 2000). Accuracy and details of CTD measurements and calibration procedure for the data collected between 1991 and 1994 are described by *Bönisch et al.* [1997]. Data collection, processing, and quality for the cruises conducted between 1995 and 2000 are similar to those reported by *Bönisch et al.* [1997] for the 1994 cruise. The overall precision of the CTD data is 0.003 K for temperature and 0.003 for salinity for 1991 and 1992 and 0.001 K and 0.002, respectively, for the 1993 to 2000 CTD data [*Blindheim and Rey*, 2004]. Temperature is reported on the International Temperature Scale 1968 (IPTS 68), and salinity is reported in practical salinity units (PSS 78).

4. Results

4.1. Vertical Distribution of Properties Along 75°N

[14] The general structure of the Greenland Sea gyre is discussed using two zonal sections occupied about 6 years apart (November 1993 and June 1999; Figure 2), nominally along 75°N. Here we focus on temperature, salinity, and the transient tracer CFC-11 to illustrate the main features and their differences between the two occupations of the section.

[15] Sections from both years show similar overall patterns. The vertical structure of the central gyre, approximately between 2°E and 6°W, can be viewed as a four-layer system associated with particular water masses.

[16] The upper layer is influenced by the local seasonal cycles in heat and freshwater fluxes, as well as lateral intrusions from the gyre rim, and extends to approximately 500 m depth. It can be identified by the depth of the lowest temperature/salinity values in the very center of the gyre. Toward the gyre rim, the stratification increases and is more and more determined by advection: In the east, warm and saline Atlantic Water is advected with the West Spitzbergen Current, and in the west, cold and fresh Arctic Water as well as warm saline return Atlantic Water is advected with the East Greenland Current. Owing to intense seasonal forcing, with variable strength of local and lateral sources, no particular water mass can be associated with the upper layer.

[17] Below the upper layer, in the intermediate layer, the integral effect of winter convection can be identified as a rather homogeneous patch of fresh and cold water. The overall lateral extent of the patch appears to be larger in June 1999 than in November 1993, but this observation might be due to the different seasons during which the cruises took place. The water mass associated with the intermediate depth range is often called Arctic Intermediate Water [e.g., *Swift and Aagaard*, 1981; *Blindheim*, 1990; *Meincke et al.*, 1997]. However, we will refer to it as Greenland Sea Intermediate Water (GSIW) to emphasize its rather local formation in the Greenland Sea and to contrast it with intermediate waters formed in the Norwegian and Iceland seas. A slight doming of the isopycnals reaches down to a depth of about 1500 m, indicating the cyclonic gyre circulation.

[18] Within the intermediate layer a subsurface temperature maximum (T_{max}) can be found [*Meincke et al.*, 1997; *Budeus et al.*, 1998]. T_{max} was located at about 1000 m depth in 1993 and at about 1500 m depth in 1999. *Meincke et al.* [1997] interpreted T_{max} to be of Arctic origin, specifically Canadian Basin Deep Water. We propose below an alternative process of local formation of T_{max}. The strongest gradient in all tracer concentrations is aligned with T_{max}. For example, the vertical gradient in CFC-11 concentration above T_{max} is weaker in 1999 than in 1993. In 1993, a local salinity maximum at the western part of the gyre at about 1400 m depth indicates a separation of water from past convective events and renewed water. Convection at the end of the 1980s had reached depths between 1600 and 2000 m [*GSP group*, 1990; *Rhein*, 1996]. In 1999, no local salinity maximum could be seen at intermediate depth, but a strong vertical gradient in salinity was present at the base of the T_{max} layer.

[19] The depth range from about 2000 to 3000 m is occupied by GSDW. GSDW is quite homogeneous in the gyre center in all properties, while horizontal gradients exist toward the gyre rim. At the rim, high-salinity cores can be seen at about 2000 m depth. They are, at least in part, of Arctic Ocean origin [*Aagaard et al.*, 1991; *Meincke et al.*, 1997; *Rudels et al.*, 2000]. Between 1993 and 1999 the homogeneous salinity layer ascended by about 300 m with an overall increase in salinity of about 0.004. Between 1993 and 1999 the vertical as well as the horizontal CFC-11 gradients below a depth of 2000 m weakened. Greenland Sea Bottom Water (GSBW) is located beneath GSDW between roughly 3000 m depth and the bottom. It is characterized by lower salinities and lower temperatures than GSDW. There is no significant change in GSBW CFC-11 content.

4.2. Temporal Variability in the Central Greenland Sea Gyre

[20] The temporal variability of hydrographic variables and transient tracer concentrations in the central Greenland

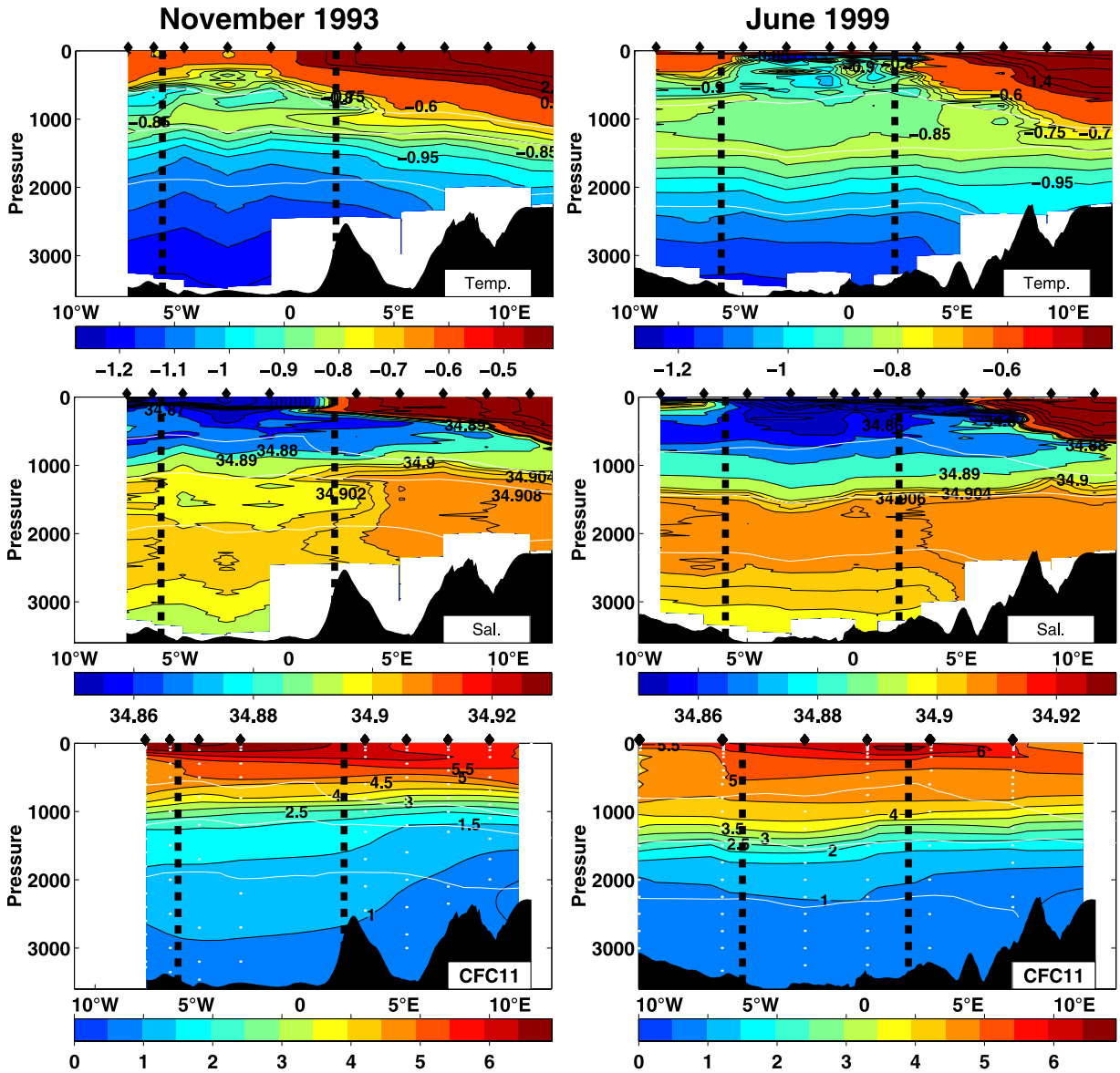

Figure 2. Sections of (top) temperature, (middle) salinity, and (bottom) CFC-11 along ~75°N in (left) November 1993 and (right) June 1999. White overlay indicates the $\sigma_{1.5}$ density anomaly contour (35.13, 35.14, 35.15), white dots in bottom panels indicate the bottle sample depth used to produce the contour plots via objective analysis, and black dots on top of figures indicate station positions. The central Greenland Sea gyre is bound by the broken lines at 6°W and 2°E, and data between these positions are used to construct the time series plotted in Figure 3. Temperature, salinity, and density contours are based on CTD data.

Sea (Figure 3; for boundaries see Figures 1 and 2) was investigated from the objectively mapped [*Roemmich*, 1983] tracer distributions. In some years a few profiles deviated strongly from the mean profile as they captured remnants of convective events. These profiles were excluded from the averaging process as they do not represent the characteristics of the gyre as a whole (mixed patch). They will be discussed separately.

4.2.1. Upper Layer

[21] The upper layer water is modified through variable air-sea exchange, sea ice formation/melting, and intensity of lateral intrusions. Having available only 10 annual snapshots of the gyre, no conclusion on temporal changes in temperature and salinity (Figures 3a and 3b) can be drawn from this coarse resolution time series in the highly variable upper layer. However, the time series of salinity and temperature allow conclusions on the approximate depth to which seasonal variability penetrates. This depth is about 500 m.

[22] In contrast to temperature and salinity, the transient tracer concentrations are less affected by seasonal variability. For example, in the very near surface (0 to 20 m), concentrations close to solubility equilibrium with the atmosphere were found for the various anthropogenic halocarbon compounds (Figure 4). On average, considering all available data (Figure 1), most of these compounds were

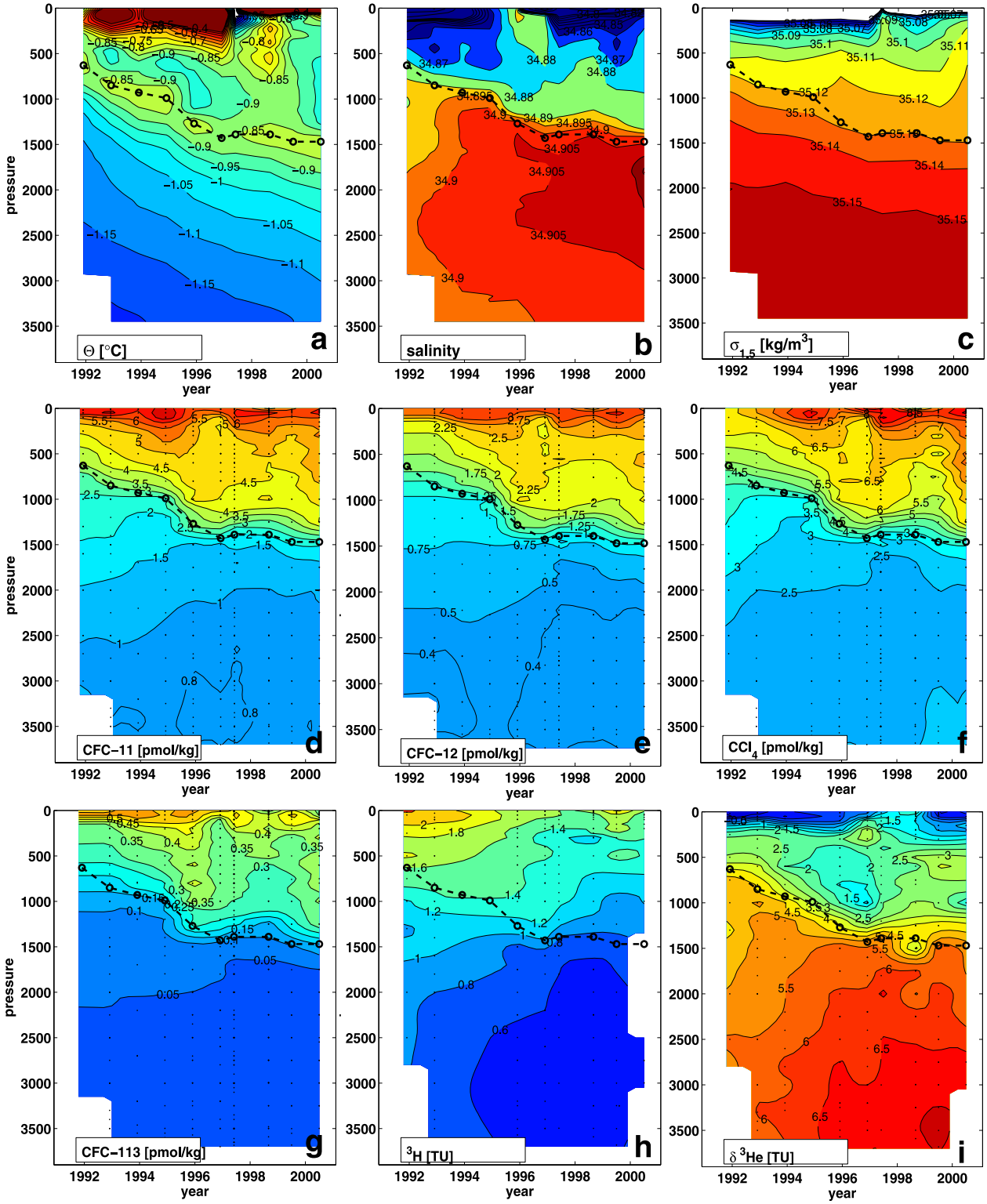

Figure 3. (a) Temperature, (b) salinity, (c) $\sigma_{1.5}$ (density anomaly reference to 1500 dbar), (d) CFC-11, (e) CFC-12, (f) CCl_4, (g) CFC-113, (h) tritium, and (i) δ^3He time series in the central Greenland Sea gyre (compare Figures 1 and 2 for location). The depth of the interior temperature maximum is indicated as a dashed line. Average profiles were constructed via spline interpolation. For color coding, see labels.

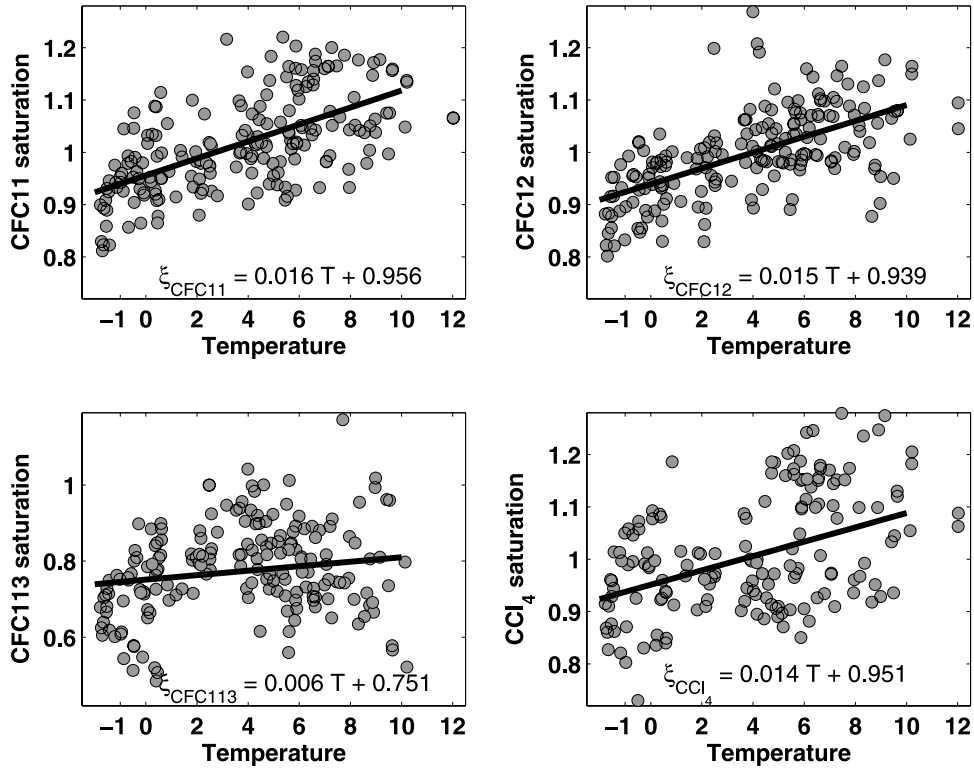

Figure 4. Saturation (ξ) of CFCs and CCl_4 in the upper (<20 m) waters of the entire sampled region as a function of temperature (T). Linear best fit and fit equations are included in the figures.

close to solubility equilibrium with the atmosphere (e.g., for CFC-11, average saturation was 100.6%). The clear exception was CFC-113, which was, on average, undersaturated. In areas with significant vertical mixing or upwelling such as the Greenland Sea gyre, the undersaturation of surface waters is partially determined by the subsurface vertical concentration profiles. The oceanic profile of CFC-113 shows a "steeper" decline with depth than that of the other tracers the concentrations of which have increased more slowly or have even become stationary over the past 2 decades (Figure 5). Hence the lower saturation of CFC-113 is most likely related to its more rapid increase in the atmosphere. There is also evidence for the nonconservative behavior of CFC-113 in seawater [*Roether et al.*, 2001], but the rate of CFC-113 removal appears to be slow in cold waters.

[23] The surface saturation (ξ) of all CFCs and CCl_4 in this region was positively correlated with temperature. The relationship between temperature and CFC-12, CFC-11 and CCl_4 (Figure 4) was very similar, and from a least squares fit we obtain the following empirical equation for the saturation as function of surface temperature (T) for the range between about −2 and 10°C:

$$\xi(\mathrm{CFC}-11, \mathrm{CFC}-12, \mathrm{CCl_4}) = (0.02 \times \mathrm{T} + 0.93) \times 100\%.$$

This relationship may be useful to prescribe the surface water saturations in modeling studies of the region, at least for summer conditions (we lack coverage during winter months).

4.2.2. GSIW Layer

[24] Below the upper layer the variation of the temperature and salinity fields reveals interannual cooling and warming signals reaching down to a depth of ∼1500 m in the year 2000. The layer hosts the intermediate depth temperature maximum (T_{max}) which deepened rather rapidly during the first half of the 1990s and leveled out at about

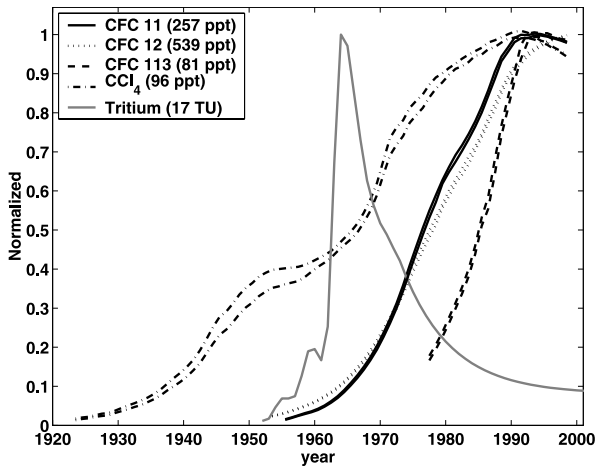

Figure 5. Input of tracers over the Northern Hemisphere and GIN seas [*Walker et al.*, 2000; *Bönisch and Schlosser*, 1995]. The numbers in the legend give the conversion factors from the actual concentration scale to the normalized scale. Double lines for CFCs indicate the uncertainty in atmospheric time histories as given by *Walker et al.* [2000].

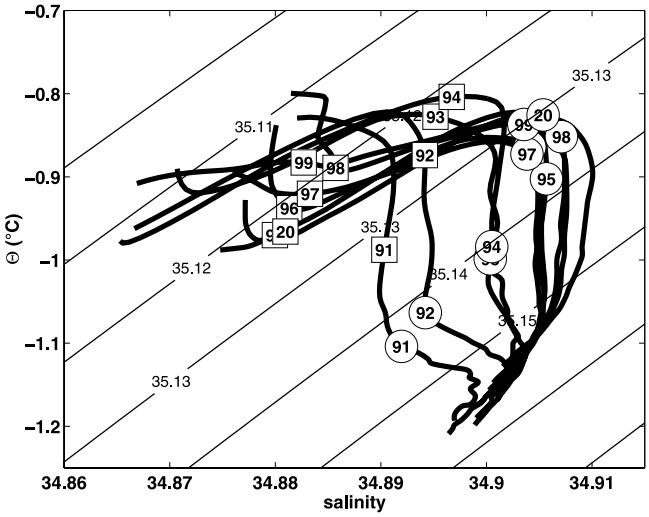

Figure 6. Temperature/salinity diagram for waters of the central Greenland Sea (74°N to 77°N and 6°W to 2°E) from spline-averaged CTD observations. Density anomaly contours (reference 1500 dbar) are shown. The squares and circles mark the depths of 600 and 1500 dbar, respectively, whereas the observational profile year when the profiles have been taken are given from 1991 (91) to 2000 (20).

1500 m in the second half. Extensive deepening of T_{max} occurred between 1991 and 1996 from about 600 to about 1500 m. In 1999/2000, another convective event took place but with no significant further deepening of T_{max} [*Karstensen et al.*, 2003]. At present (year 2005), T_{max} is located somewhat deeper, at about 1800 m depth. According to the temperature/salinity diagram (Figure 6) the hydrographic properties changed quite dramatically in the intermediate layer. At 600 m depth (squares in Figure 6) a warming and slight salinity increase with change in density occurred from 1991 to 1994 during the rapid descent of T_{max}. Between 1994 and 1995 an intense cooling and freshening followed, but with little change in density. In later years both warming and cooling periods occurred with little change in salinity, nearly preserving density. At 1500 m depth (circles in Figure 6) an overall warming trend accompanied by a salinity increase can be identified with changes in density occurring after 1995. The T/S characteristics of T_{max} are rather constant since 1995 (Figure 6) with a temperature of about −0.9°C and a salinity of 34.904.

[25] Examination of the historical database for this region [*Bönisch et al.*, 1997] reveals earlier periods (end of 1950s) during which a T_{max} layer can be observed. However, identification of this feature in early data sets is problematic because it was poorly resolved by bottle and reversing-thermometer data sets. *Budeus et al.* [1998] used a linear extrapolation of the deepening of T_{max} between 1993 and 1996 (of the order of 150 m y^{-1}) to estimate the period of time required for renewal of the deep waters to be about 20 to 30 years. In view of the slowing of deepening in recent years, however, such predicted renewal times of GSDW may be too short.

[26] The T_{max} layer developed at the end of the 1980s/early 1990s [*Budeus et al.*, 1998] and aligns in all tracer data sets (Figure 3) with rather strong vertical gradients around the T_{max} core. Increasing tracer inventories above T_{max} suggest that the deepening is linked to convective events [*Karstensen et al.*, 2003]. Convection, however, is limited to depths above T_{max} as this layer would otherwise erode. We interpret T_{max} as the deepest separation horizon of waters renewed during the 1990s through the local air-sea-ice interaction from "older" water.

[27] A strong salinity gradient is associated with T_{max} and descended in pace with the deepening of T_{max} to finally (in 2000) merge with the salinity maximum at 2400 m, which originates in the Arctic Ocean [*Meincke et al.*, 1997]. Thus a broad salinity maximum reaching from 1500 m to 2400 m depth was present at the end of our time series. This broad salinity maximum has consequences for further deep convection as will be discussed below.

4.2.3. Deep and Bottom Water Layers

[28] In the GSDW/GSBW layer the temperature and salinity (at constant depth) increased during the 1990s. These changes are consistent with lateral mixing of Arctic Ocean Water from the gyre rim [*Aagaard et al.*, 1991; *Meincke et al.*, 1997] (see also Figure 2) as well as with mixing of water from the intermediate layer [e.g., *Visbeck and Rhein*, 2000]. Although Arctic Ocean Water would spread into the Greenland Sea along isopycnals above the sill depth of Fram Strait (∼2600 m), it can reach greater depths and even the bottom as a consequence of diapycnal vertical transfer in the boundary layer [*Aagaard et al.*, 1991; *Visbeck and Rhein*, 2000]. To interpret the evolution of transient tracers in GSDW and GSBW, one has to carefully consider the uncertainties associated with the data which will be done in greater detail in section 5.2.

5. Discussion

5.1. GSIW and the Evolution of the T_{max} Layer

[29] The most striking feature in the transformation and renewal of water masses in the Greenland Sea gyre during the 1990s was the occurrence and deepening of T_{max}. Although subsurface temperature maxima occur in other regions of deep convection such as the Labrador Sea, the persistence of T_{max} in the Greenland Sea is remarkable.

[30] In contrast to earlier work [*Meincke et al.*, 1997; *Budeus et al.*, 1998], we explain the generation of T_{max} by the convection process itself, in particular through a thermally driven convection but with an anomalous high addition of freshwater. Convection is mainly a vertical process (see *Marshall and Schott* [1999] for a review). Surface water is densified through cooling and/or salinification driven by air-sea-(ice) exchange and subsequently sinks. During sinking the underlying water is entrained, altering the properties of the descending plume. A homogeneously mixed patch composed of "young" sinking and "old" entrained gyre water is created [*Send and Marshall*, 1995]. If the convection is driven through a thermal buoyancy loss but with a parallel gain in buoyancy due to the presence of a freshwater source, the renewed water would be colder than the old (before convection) gyre water. Although colder, the overall density of the water may not increase owing to its lower salinity. If we further assume that the old gyre water decreased in temperature with depth, as observed at the end of the 1980s in the Greenland Sea,

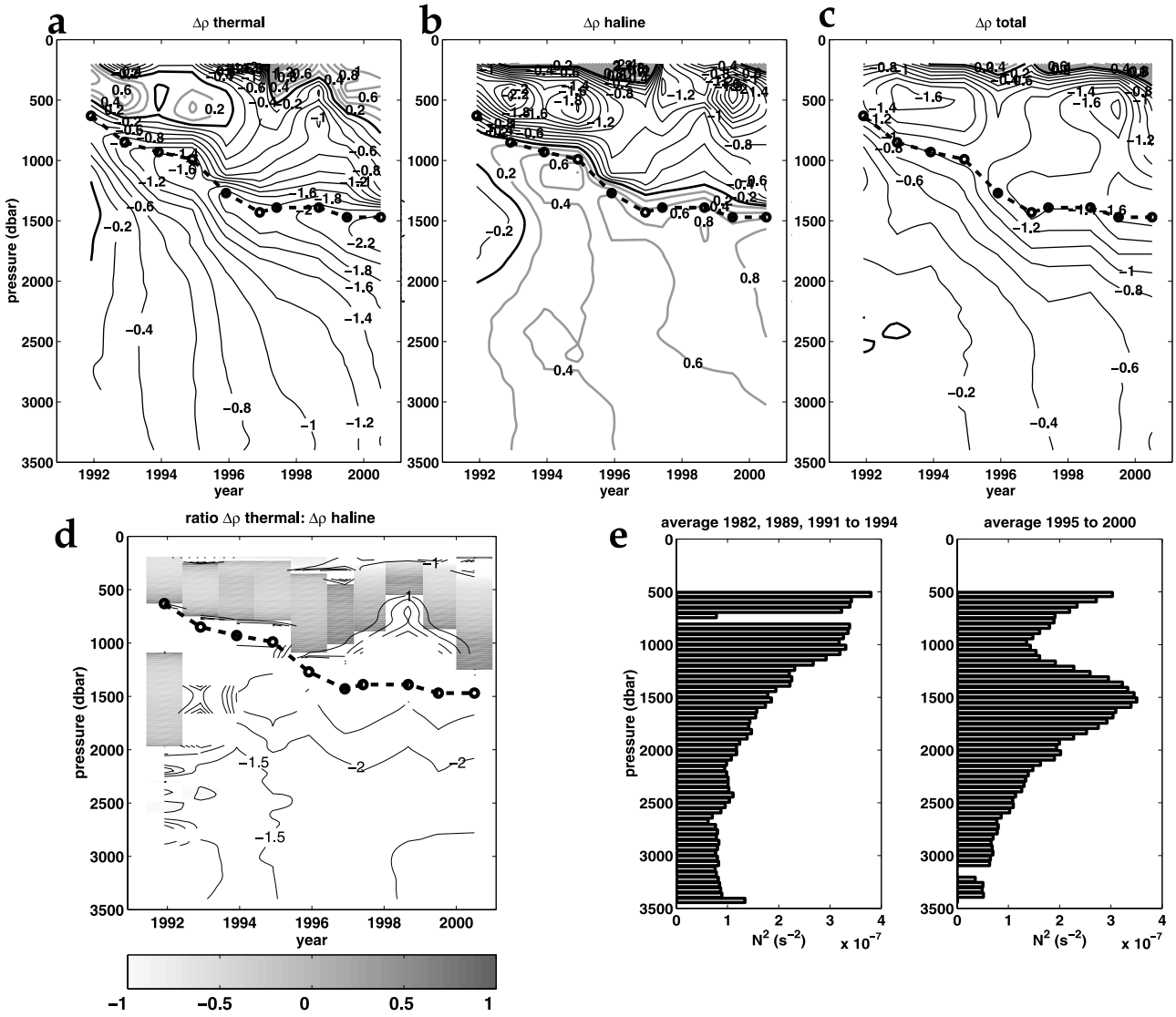

Figure 7. (a) Thermal, (b) haline, (c) total (sum of thermal and haline) density changes (in 10^{-5} kg m^{-3}), and (d) the ratio of thermal versus haline changes (range −3 to 3 only) in the central Greenland Sea. The 1989 data from the Greenland Sea Project [GSP group, 1990] were used as a reference point. In Figures 7a to 7c, shaded lines are used to indicate density gain, and black lines indicate density loss. In Figure 7d the shading indicates dominance of the haline density change on the total density change. The broken line in Figures 7a to 7d indicates the locations of T_{max}. (e) Stability ($N^2 = -(g/\sigma_0)\partial\sigma/\partial z$) in the central Greenland Sea gyre between 500 and 3500 m depth averaged for data (left) before 1995 and (right) after 1995.

the convection process would form a T_{max} layer at the base of the mixed patch, as a remnant of the gyre stratification before convection. Another prerequisite for the formation of a stable T_{max} layer is an appropriate initial salinity stratification, which would be an increase in salinity with depth, again, such an increase was found in the Greenland Sea at the end of the 1980s.

[31] To elucidate the interplay between the temporal temperature and salinity changes on the density changes in the Greenland Sea during the 1990s, we separated their effect using a linearized equation of state,

$$\rho = \rho_0[1 - \alpha(T - T_0) + \beta(S - S_0)],$$

where $\alpha = 1/\rho_0 \partial\rho/\partial T$ and $\beta = 1/\rho_0 \partial\rho/\partial S$. α and β are calculated from temperature, salinity, and pressure [*McDougall*, 1987]. Using the 1989 Greenland Sea Project [*GSP group*, 1990] data as the reference stratification (T_0, S_0), the individual contribution of temperature and salinity (Figures 7a and 7b), as well as their combined effect on the density changes, are calculated (Figures 7c and 7d).

[32] Overall, there is a decrease in density throughout the entire water column if referenced to 1989 (Figure 7c). As seen in the tracer time series, the hydrographic changes in the upper 500 m are dominated by seasonal variability and cannot be interpreted using our coarse resolution time series. The intermediate waters have a two-layered structure: Above T_{max}, both the thermal and haline components

decrease the density through warming and freshening, respectively. However, in the upper part of the intermediate layer the freshening dominates the density changes. This is evident from the ratio of thermally to haline driven changes (scale between −1 and 1). Below T_{max} the increase in salinity compensates in part for the warming. This effect is particularly effective at depths where the intermediate waters merge with waters characterized by a salinity maximum derived from the Arctic Ocean (located at ~2400 m depth [*Aagaard et al.*, 1991; *Meincke et al.*, 1997]). As a consequence, the largest salinity driven density increase can be found at a depth of about 2000 m in 2000. In the Deep and Bottom Water, the density decrease due to warming outweighs the density increase from salinity increase by about a factor of 2. The net effect in the Deep and Bottom Water is a density loss with respect to the 1989 reference profile. In the year 2000, the maximum combined density change (at about 1300 m) is of the order of $\Delta\rho = -1.5 \times 10^{-5}$ kg m^{-3} if referenced to the 1989 profile. To compensate such a density decrease, a 0.02 higher salinity (using $\beta = 7.7 \times 10^{-4}$) or 0.19°C lower temperature (using $\alpha = 78 \times 10^{-5}$ K^{-1}) would be required.

[33] Above T_{max} the main contributor to the density decrease is in the haline component. The freshwater required to lower the salinity probably entered the intermediate layer during the first half of the 1990s. By using the salinity change between 1989 (S_{1989}) and the observations from 1991 to 2000 (S_{obs}), the annual average freshwater flux ($F_{S=0}$) from the upper layer to the intermediate can be calculated considering the volume of the central Greenland Sea gyre (VGS; radius 1.2×10^5 m):

$$F_{S=0} = (S_{1989}/S_{obs} - 1) \times VGS. \quad (1)$$

For the depth range 500 to 1500 m, on average, the salinity was lower by 0.006 during the 1990s compared to 1989. Using equation (1) this translates into a total freshwater increase of about 1×10^{11} m^3 (100 km^3; equivalent to the addition of ~2 m of freshwater to the surface of the GS). As discussed above, the freshwater import is a prerequisite to establish a T_{max}, and we suspect that the freshwater anomaly (in reference to 1989) was established at the beginning of the 1990s. The Arctic Ocean is the largest freshwater source for the GIN seas and is the likely source for this increase. *Aagaard and Carmack* [1989] give a GIN seas annual mean freshwater gain through export from the Arctic of about 1×10^{12} m^3, which is an order of magnitude larger than what we obtained from our rough calculation. An increased export of freshwater from the Arctic Ocean at the end of the 1980s and extending into the 1990s is consistent with model results on the interannual variability of the Arctic sea-ice volume [*Köberle and Gerdes*, 2003; M. Karcher et al., personal communication, 2004] and further supports an Arctic Ocean origin of the anomalous freshwater increase in the Greenland Sea intermediate layer.

[34] T_{max} has not been eroded during its descent in the Greenland Sea water column during the 1990s, and consequently this deepening has implications for the dynamics of the gyre. For T_{max} to sink, water below T_{max} has to be exported from the gyre. From Figure 3 we estimate that the deepening of T_{max} was about 1000 m over 10 years, equivalent to a vertical velocity of about 3×10^{-6} m s^{-1}, with a rather constant deepening during the first half of the decade. Assuming a gyre radius of 1.2×10^5 m, the export of water from the layers below T_{max} is of the order of 0.1 Sv (possibly up to 0.2 Sv considering that most of the deepening took place during the first half of the decade). This rate is similar to tracer-derived water mass formation rate estimates for the upper layer [*Rhein*, 1996; *Karstensen et al.*, 2003]. However, such rates have to be seen as lower bounds of water mass formation because they do not consider the export of water during convection or restratification.

[35] The lateral export of water could also be a reason why T_{max} is no longer descending as rapidly as it did at the beginning of the 1990s [*Budeus et al.*, 1998]: The ridges that separate the Greenland Sea from the Norwegian and Iceland Sea have sill depths of about 1800 m which may prevent the lateral export and hence the sinking of T_{max}.

[36] A further dynamical constraint on the sinking of T_{max} is imposed by the potential vorticity (PV) of the gyre. PV combines information on stratification and flow and, under certain conditions, is a conservative tracer of a water mass [e.g., *Keffer*, 1985]. To address the changes in the Greenland Sea, we approximate the gyre as a cylinder with two layers, separated at the depth of T_{max}. The upper layer is exposed to air-sea exchange, and no conservation of vorticity can be postulated. For the lower layer, however, conservation of PV may be assumed. PV can be written as the sum of planetary vorticity f (about 1.4×10^{-4} s^{-1}) and relative or shear vorticity (ζ), considering the height (H) of a water column [e.g., *Pond and Pickard*, 1983],

$$PV = (f + \zeta)/H = \text{const.} \quad (2)$$

A deepening of T_{max} (squeezing of the lower layer) evokes a negative ζ or anticyclonic vorticity. For convenience, we estimate the magnitude of ζ as a fraction (n_f) of the planetary vorticity f assuming the initial PV has $\zeta = 0$. Considering that PV has the same value before (H_1) and after (H_2) deepening of T_{max}, we rewrite equation (2) to obtain n_f as

$$n_f = H_2/H_1 - 1.$$

[37] Using the deepening from about 500 m depth in 1991 (H_1 = 3000 m) to 1500 m in 2000 (H_2 = 2000 m) we obtain $n_f = -0.3$ or ζ would be 30% of $-f$. This is apparently a very high value for ζ but typical for deep convective eddies [*Gascard et al.*, 2002] which frequently occur in the region and, as discussed below, are found in our data as well.

[38] During the descent of T_{max}, there is a warming and salinity increase of that layer. It not only lowers its density (Figure 3), but changes the vertical density gradient (Figure 7). Using an alternate formulation for PV that considers the potential density (ρ_Θ) stratification [e.g., *Keffer*, 1985],

$$PV = -f\rho_\Theta^{-1}(\partial\rho_\Theta/\partial z),$$

allows us to obtain further insight into the dynamics of the deepening. The average density profiles of the central gyre show the most dramatic changes in stability (expressed in

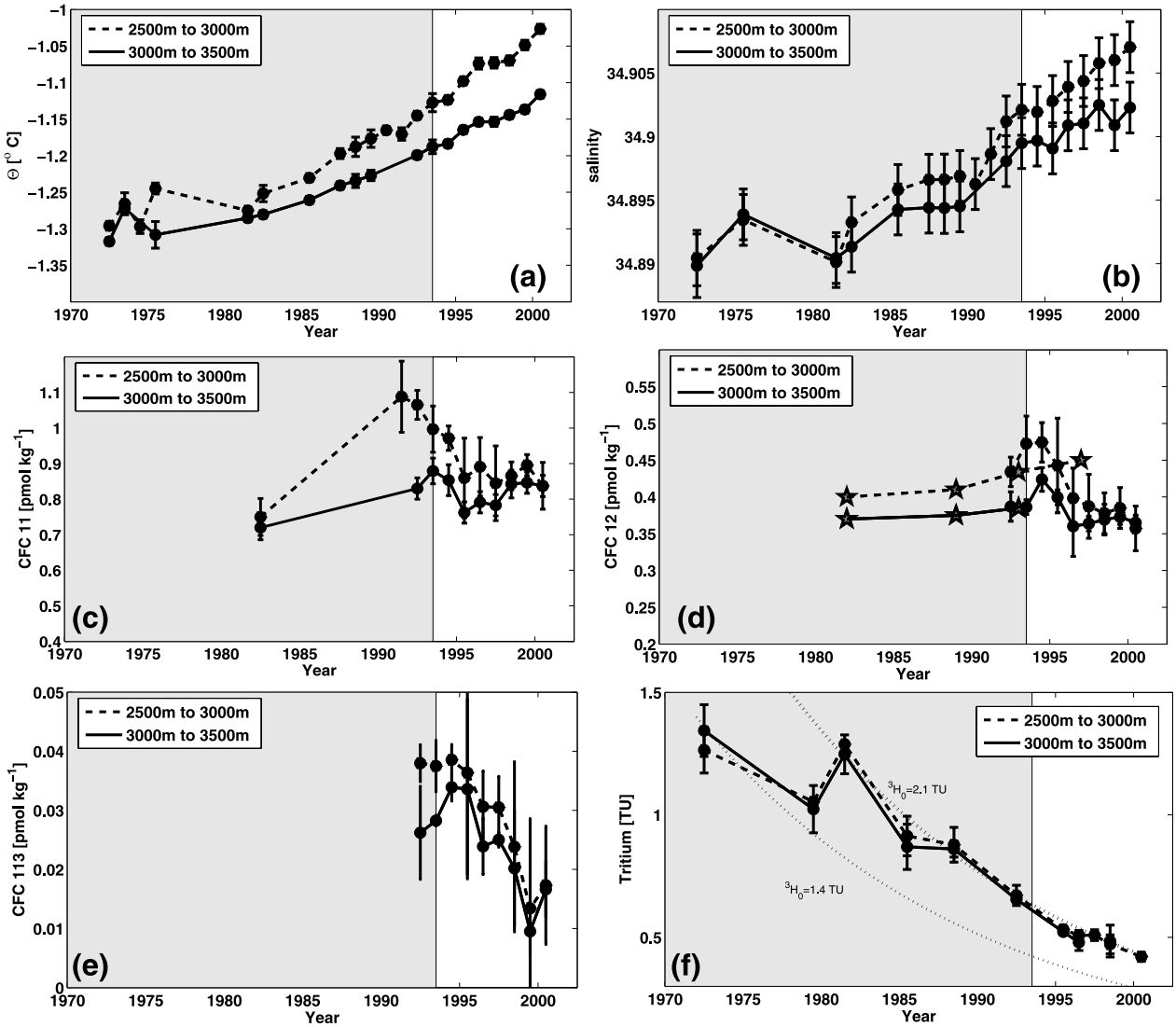

Figure 8. Evolution of central Greenland Sea gyre Deep Water (2500 m to 3000 m) and Bottom Water (3000 m to 3500 m) mean properties and accompanied standard deviation (based on scatter in the observations): (a) temperature, (b) salinity, (c) CFC-11, (d) CFC-12 (stars mark values of *Visbeck and Rhein* [2000]), (e) CFC-113, and (f) tritium. The dashed lines in Figure 8f are the radioactive decay of tritium starting with the arbitrary concentrations 2.1 TU and 1.4 TU in 1970. Other data before 1991 are reported by *Bönisch et al.* [1997]. The time interval before 1994 is shaded.

terms of buoyancy frequency in Figure 7e) between 1994 and 1995. These particular years are important as during that time not only a temperature anomaly (T_{max}) descended but the deep salinity maximum related to the core of the Arctic Ocean water salinity (core depth: ~2400 m) merged with the small salinity maximum (strong gradient) that was lowered in the water column along with the deepening of T_{max}. This evoked a change in the vertical density stratification to a depth of about 2200 m (Figure 7c) and established a broad stability maximum centered at about 1500 m (Figure 7e). In view of the PV changes for the lower layer we conclude that the increase in ζ of $\sim -0.3\ f$ was compensated by a "major" restratification of the water column. We note that major restratification has to been seen in light of the general very weak vertical stratification of the gyre. We further note that below 2200 m the temperature and salinity changes cause a rather homogeneous density change with depth that does not change the vertical density gradient and hence do not change the stability nor PV (Figure 7e). Using density and velocity finestructure CTD and lADCP measurements, *Naveira Garabato et al.* [2004] recently showed that the stability maximum associated with T_{max} coincides with a minimum in dissipation rate and vertical mixing.

5.2. Deep Water Changes

[39] *Bönisch et al.* [1997] discussed the temporal evolution of the deep waters on the basis of historical and recent data up to 1994. Here we construct for the lower part of the Deep Water (2500 to 3000 m) and Bottom Water (3000 to 3500 m) time series utilizing the *Bönisch et al.* [1997] data but adding data from 1995 to 2000 (Figure 8). The rather

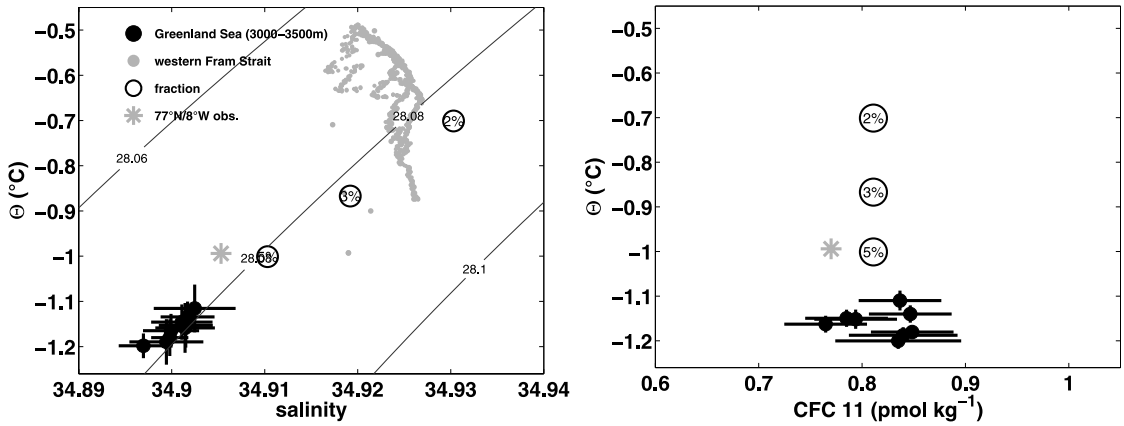

Figure 9. Deep Water box model (left) Θ/S pairs and (right) Θ/CFC-11 pairs that would satisfy the observed changes in the deep central Greenland Sea (3000 to 3500 m depth). The observational data from the central Greenland Sea (black dots) and the observations from western Fram Strait (shaded dots are CTD data, shaded star is 1997 bottle data (T. Tanuha, personal communication, 2003) are included. The open circles denote the amount of admixture (in percent) of a certain Θ/S and Θ/CFC-11 pair that would explain the observed trend in the deep Greenland Sea in reference to the 1992 data. See text for details.

linear increase in temperature (0.01 K yr^{-1}) and salinity (0.001 yr^{-1}) holds for the last 3 decades (Figures 8a and 8b). There might, however, be a divergence of the curves, implying a more rapid warming and salinification of the Deep Water compared to the Bottom Water.

[40] Depth-averaged concentrations of CFC-11 and CFC-12 in GSDW increased up to 1993 followed by a pronounced decrease in the following 2–3 years. GSBW concentrations followed this trend, but at lower concentrations. The merging of GSDW and GSBW CFC concentrations indicates a decrease in the vertical gradient between 2000 m depth and the bottom. CFC-113 shows a pronounced decrease between 1993 and 1999. We interpret the decrease in CFC's since 1993/1994 as a decoupling of the intermediate and deep layers and attribute it to the deepening of the stability maximum associated with T_{max}. The stability maximum reduces the vertical exchange with the intermediate layer and allows for an increased role of admixture of Arctic Ocean Deep Waters (AODW) in the renewal of the deep and bottom waters. As we expect AODW to be more depleted in CFC-113 owing to its more recent history in the ocean (CFC-113 was introduced about 20 years after CFC-11 and CFC-12; see Figure 5) mixing with AODW will decrease the CFC-113 content stronger than the CFC-11 or CFC-12 concentrations. Since the mid-1980s, tritium decreased at a rate very close to that expected from radioactive decay (Figure 8f). This is similar to a practically linear increase in tritium/^{3}He age [see *Bönisch et al.*, 1997]. Again, this would be in line with adding AODW of similar tritium concentration to the Deep and Bottom Waters. Before the mid-1980s, tritium concentrations increased as a result of water mass renewal [*Schlosser et al.*, 1991].

[41] *Visbeck and Rhein* [2000] proposed a GSDW increase in CFC-12 through enhanced vertical mixing of water from the intermediate layer, based on CFC-12 observations in 1982, 1989, 1993, and 1997. Except for the 1997 data, the *Visbeck and Rhein* [2000] observations below 2500 m (stars in Figure 8d) agree well with our data. Possible reasons for the higher CFC-12 values in the 1997 [*Visbeck and Rhein*, 2000] data could be: (1) including data at the level of T_{max} (1500 to 2500 m) in their analysis, or (2) including data measured in a small-scale feature not representative for the gyre as a whole [*Visbeck and Rhein*, 2000, Figures 4b and 4c].

[42] CFC-11, CFC-12 and tritium have been delivered to the ocean in significant amounts since about the beginning of the 1960s (Figure 5). Although AODW has reached significant transient tracer concentrations [e.g., *Bönisch and Schlosser*, 1995], these concentrations are still lower than those observed in GSDW and GSBW. Consequently, mixing of AODW and GSDW does not increase the tracer concentrations of GSDW or GSBW. On the other hand, if GS water from intermediate depth would be added to Deep and Bottom Waters, its CFC content would significantly increase while its tritium content would be affected much less because the surface tritium concentrations have decreased over time and presently are relatively low. Therefore the increase in CFCs during the 1980s and the beginning of the 1990s is interpreted as renewal that involves vertical mixing as well as admixture of water from the Arctic. After 1994 the decrease in both CFCs and tritium are consistent with admixture of AODW without significant addition of GSIW.

5.3. Connection to Adjacent Seas

[43] If we extrapolate the temperature and salinity trends observed in GSDW and GSBW into the future, it will take roughly 20 years for the deep Greenland Sea to reach Arctic Ocean Deep Water characteristics (Θ = −0.8°C, S = 34.937) unless new local Bottom Water formation takes place. Utilizing the Bottom Water temperature, salinity, and CFC-11 characteristics, we calculated the annual contributions of a "virtual water mass" which would have to be added to GSDW and GSBW to produce the observed trends in the properties of these water masses during the 1990s (Figure 9). We use observations from western Fram Strait as properties for this "virtual" water mass. From the Θ/S data of the virtual water mass the observed changes in GSBW are

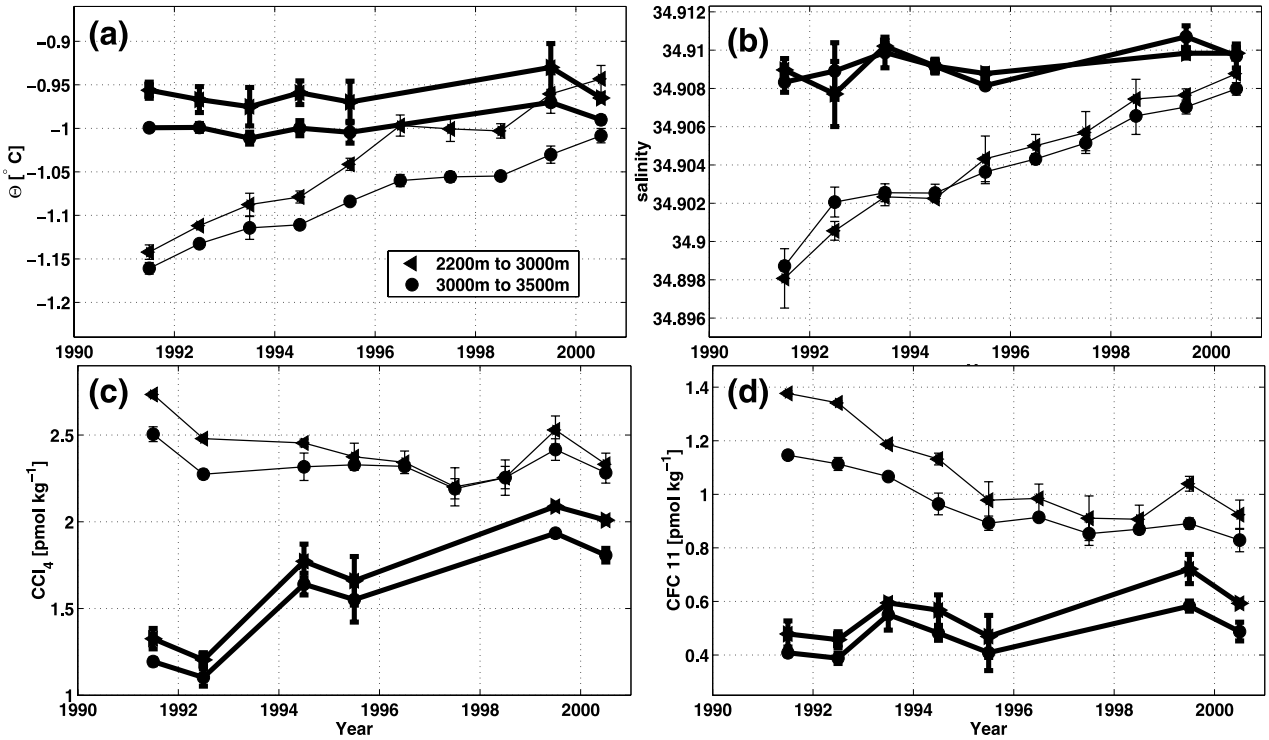

Figure 10. Comparison of the temporal evolution of the tracer data from the central Greenland Sea (thin black lines) and the central Norwegian Sea (thick black lines) for the depth range 1900 to 2200 m and 2200 to 2500 m. See Figure 1 for regional separations. Note that the depth range is different than the one used in Figure 8.

consistent with an annual admixture of 2 to 3% of Arctic Ocean Water, confirming the results by *Anderson et al.* [1999]. For CFC-11, no real trend in the GSBW can be seen, and we expect that the water that enters from the Arctic has CFC-11 concentrations similar to those of GSBW. This scenario is supported by CFC-11 data collected at the Greenland Sea side of Fram Strait (77°N/8°W; T. Tanuha, personal communication, 2003), although these data suggest a higher admixture of about 5%.

[44] The warming and salinification of the deep Greenland Sea could have an impact on the deep circulation in the Arctic Mediterranean, as it would preclude the heat and salt loss of Arctic Ocean Water to GSDW and GSBW. As Arctic Ocean Water contributes directly to the Denmark Strait overflow water, a change in the overflow characteristics is a likely consequence.

[45] As the deep Greenland Sea waters contribute to the ventilation of the deep Norwegian Sea [*Smethie et al.*, 1986; *Swift and Koltermann*, 1988], a warming and salinification trend of the gyre could also impact the exchange with the Norwegian Sea [*Osterhus and Gammelsrod*, 1999]. For the period between 1984 and 1997, *Rudels et al.* [2000] found a similar warming (0.1°C) and salinity increase (0.013) at the sill depth of Fram Strait. Our station coverage in the Norwegian Sea gyre is sparser than that for the Greenland Sea gyre. Using available data from the Lofoton Basin of the Norwegian Sea, we compared average profiles 300 m above and below Mohns Ridge sill depth (2200 m; Figure 10) with data from the same depth range in the Greenland Sea gyre. Again, a local spline interpolation technique [*Akima*, 1970] was used to generate central gyre average profiles.

[46] As can be seen from all tracers, the contrast between the Lofoton basin of the Norwegian Sea and the Greenland Sea has decreased over time. This is of particular importance for temperature and salinity as they determine the pressure gradient that evokes the exchange between the two basins. The rather large volume of homogeneous Norwegian Sea Deep Water is assumed to be formed from Greenland Sea Deep Water and Arctic Ocean Water [*Smethie et al.*, 1986; *Swift and Koltermann*, 1988; *Heinze et al.*, 1990]. Owing to its larger volume, it will take longer to change the properties of Norwegian Sea compared to the Greenland Sea. As a consequence, the Greenland Sea warms much more rapidly than the Norwegian Sea, and it seems likely that the NSDW will soon be colder than GSDW and GSBW. As a consequence, a change in the flow direction from the Norwegian into the Greenland Sea is possible. Such a flow reversal was reported from current meter measurements in the Jan Mayen Fracture Zone by [*Osterhus and Gammelsrod*, 1999].

5.4. Small-Scale Features

[47] Convection regions are known to be populated with small-scale features, convective chimneys, or coherent vortices (CV) that occur on scales of the local Rossby radius [e.g., *Marshall and Schott*, 1999; *Gascard et al.*, 2002]. They are generated by baroclinic instabilities at the gyre rim where they function as horizontal mixing agents that effectively distribute water between the mixed patch and the

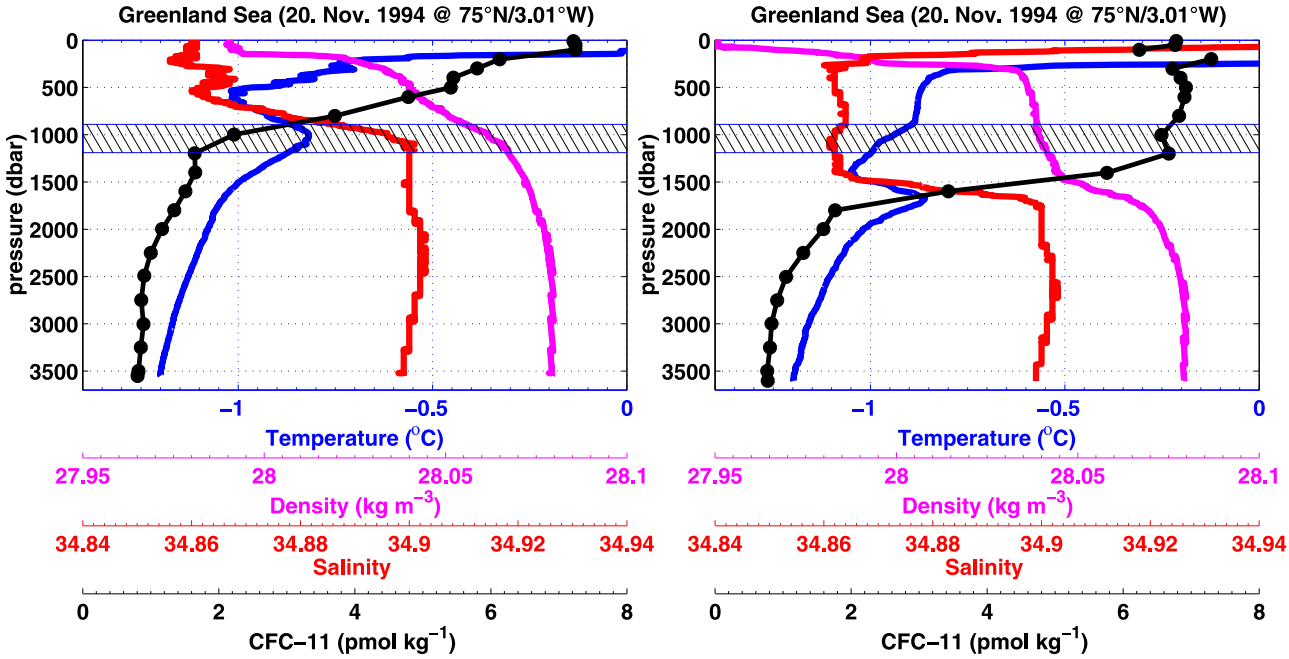

Figure 11. Example of multitracer profiles (left) of the "background" stratification and (right) within a coherent vortice in November 1994. Note not only the existence of the temperature maximum (T_{max}) but also its depth difference between large-scale patch (~1000 m depth) and the small-scale feature (~1700 m depth).

stratified waters. CVs are frequently observed in the Greenland Sea, and some appear to survive several months and possibly years [*Wadhams et al.*, 2002; *Gascard et al.*, 2002].

[48] The CVs we found in our data have a structure similar to that of the overall gyre, in particular a T_{max} at their base (Figure 11). They reach as much as 700 m deeper into the water column than the mixed patch. As in the case of the mixed patch, the temperature (and stability) maximum at their base suggest that their deepening is a nonpenetrative process, as we would expect T_{max} to be eroded during the deepening process. The T_{max} at the base of a CV is an imprint of the old gyre stratification and cannot be formed through lateral advection from the gyre rim. Moreover, it can be expected that similar physical processes drive the deepening within a CV and the gyre as a whole. As none of our data sets was collected during the winter season when active convection and hence generation of CVs takes place, they need to have a lifetime of at least several months, confirming results by *Gascard et al.* [2002]. The T_{max} underneath the mixed patch is a feature that occurred in Greenland Sea during the 1990s, and we expect that the CVs developed out of the mixed patch and hence they cannot be older than 3 to 4 years. The depth of T_{max} in the gyre and the CVs identified in our data are summarized in Table 2. *Wadhams et al.* [2002] report further details on the location and mean life time of a particular CV which had a similar T_{max} structure at its base.

[49] CVs identified in our data include colder and less saline water with higher CFC concentrations compared to the ambient water. This means that they provide anomalous properties to waters below the base of the mixed patch. However, the lateral exchange with the ambient water appears to be limited, probably as a consequence of the dynamics/rotation of the CVs. This may also explain their rather long lifetimes. From our few CV stations, it appears that density in the CVs was higher in 1993 and 1997 than in 1994.

5.5. Atmospheric Forcing and Interior Changes in the Greenland Sea Gyre

[50] Convection in the Greenland Sea gyre is largely controlled by upper layer stratification and local wind and buoyancy forcing at the air-sea-ice interface. In turn, the upper layer stratification is controlled by subsurface penetration of Atlantic Water, leakage of freshwater from the East Greenland Current, local heat, and freshwater forcing and local sea-ice formation. Our observations do not have the appropriate temporal and spatial resolution to study the processes determining the stratification in the upper water layer. However, we can discuss some potentially important forcing mechanisms using other data sources: the wind field, the surface buoyancy forcing, and the local sea-ice formation (and melting).

[51] To explore if and how the renewal might be related to local forcing at the air-sea interface, time series of heat flux and wind stress curl based on NCEP/NCAR reanalysis data were constructed for the period 1950 to 2001 (Figure 12,

Table 2. Summary of T_{max} Depth at Stations Where Coherent Vortices (CV) Have Been Detected

Station Number	Cruise Date, mm/yyyy	CV T_{max}, m	Mixed Patch T_{max}, m
1133	11/1993	1300	950
1032	11/1994	1700	1050
422, 443	04/1997	2200	1500

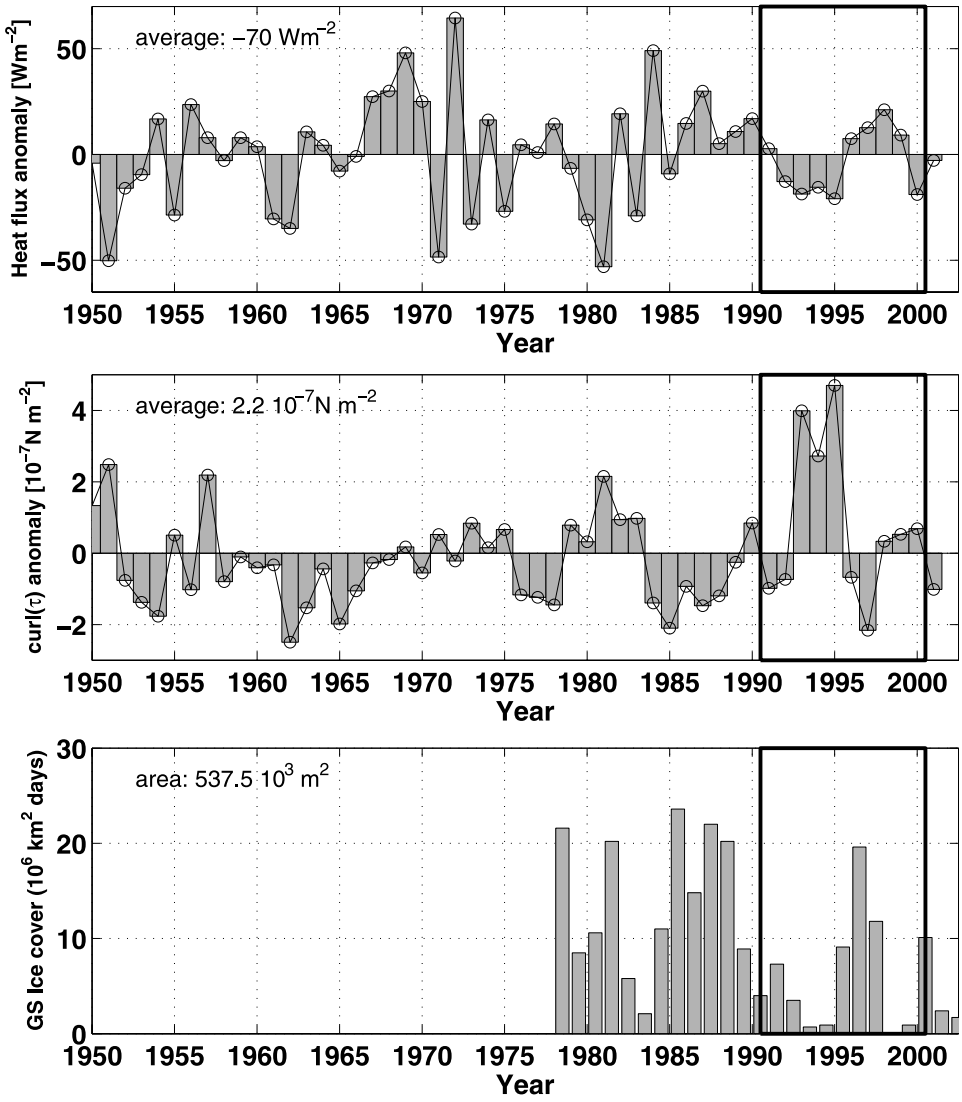

Figure 12. Annual (top) heat flux anomaly and (middle) wind stress curl anomaly based on NCEP/NCAR reanalysis data (73.3°N to 77.1°N; 5.6°W to 1.8°E). (bottom) Integrated sea-ice cover of Greenland Sea after L. Toudal (personal communication, 1999). The 1990s are framed.

top and middle). As pointed out by *Renfrew et al.* [2002] on the basis of an analysis of Labrador Sea air-sea interaction, the sensible and latent heat fluxes from the NCEP/NCAR reanalysis project are questionable. *Smith et al.* [2001] found a bias of about 20 W m^{-2} in sensible and latent heat fluxes for the entire data set. However, for our study of the relationship between changes in the surface forcing and convection activity, we are primarily interested in the relative change in the forcing rather than in the absolute flux numbers. Monthly mean NCEP/NCAR data were used to address the "memory" of the gyre resulting from long-term forcing. We expect short fluctuations to be most important for triggering small-scale individual convective events rather than the deepening of the gyre as a whole. Annual mean net heat flux and wind stress curl anomalies are derived relative to the average monthly values of the period 1950 to 2001.

[52] Between 1950 and 2001 the average annual heat loss over the gyre was about 70 W m^{-2}, and it was forced by a positive wind stress curl of about 2.3 $\times$ 10^{-7} N m^{-2}. As discussed above, the deepening of T_{max} was strongest between 1993 and 1995. It is evident that during this period the annual mean heat loss was above average (Figure 12), and wind stress curl was 3 times the mean. This supports our assumption that the deepening was initiated by intense convection that did not erode T_{max} but allowed for its downward displacement in the water column. In addition, the intensive wind stress curl may have led to strong upward tilting of isopycnals which may have slumped downward in summer as part of the seasonal cycle, thereby "pumping" isopycnals down. In the winter of 1999/2000, heat loss was also large and the tracer data suggest that convection reached down to more than 1000 m depth, but no significant further deepening of T_{max} was observed. However, wind stress curl was not strong and, as mentioned above, topography may obstruct the lateral export of water underneath T_{max}, preventing a further descent.

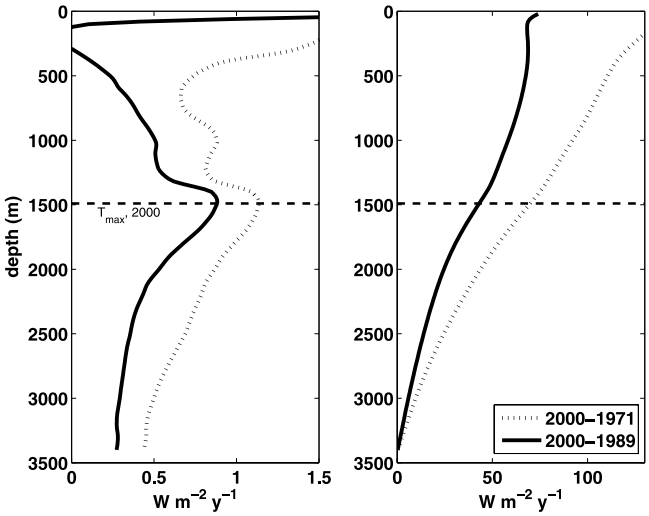

Figure 13. (left) Annual mean heat loss required to bring the system back to its 1989 and 1971 state for each 50 m depth interval. (right) Cumulative sum of the heat flux required to bring the system back to its 1989 and 1971 state referenced to the water at 3400 m depth.

[53] The local sea-ice concentrations can be reconstructed from satellite observations. *Toudal* [1999] used passive microwave observations to derive a temporally and spatially integrated amount of sea-ice for the area between about 68°N to 77°N and 10°E to 15°W (Figure 12, bottom). In this area the local sea-ice formation is particularly strong during certain years and may extend far into the central Greenland Sea to form the so-called "Is Odden." The satellite data do not allow us to distinguish between local sea-ice formation and sea-ice advection via the EGC which is of importance for the local salt balance as only the locally formed and subsequently exported sea-ice can significantly contribute to brine release [*Wilkinson and Wadhams*, 2003].

[54] Nevertheless, the sea-ice cover by itself provides useful information because it allows us to judge whether sea-ice "isolated" the ocean from intense air-sea exchange. At the beginning of the 1990s, sea-ice was nearly absent in the GS and little "isolation" and low brine release would have taken place (Figure 12). This supports thermally driven convection and a fresh surface layer, prerequisites for the formation of T_{max}. In addition, the sea-ice export through Fram Strait was particularly strong during the first half of the 1990s [*Kwok and Rothrock*, 1999; *Köberle and Gerdes*, 2003].

[55] The temperature change over time on isobars (Figure 3a) allows us to estimate the change in the gyre's heat content (Figure 13) which can be used to obtain an independent estimate of the heat flux if normalized to the area of the Greenland Sea gyre. For this estimate, we used data from 1989 and 1971 as a reference. The calculations were performed for depth intervals of 50 m using the spatially averaged temperature profiles. The cumulative sum of heat loss, starting at 3400 m depth, is shown as well. We view these numbers as the approximate annual mean heat loss that is required to bring the water column back to its 1989 and 1971 state, respectively. For the 1989 reference, we obtained the following results: GSBW (3000 to 3500 m) is affected by a rather constant warming during the 1990s and the heat gain related to this warming could be removed by an annual heat loss of the order of 5 W m^{-2} (Figure 13). From the bottom to the T_{max} layer (1500 m in year 2000), about 43 W m^{-2} of annual heat loss is required to "reset" the system. Considering the entire water column between 500 and 3400 m, a flux of about 65 W m^{-2} is required to reset the system to its 1989 heat content. These values change to about 110 W m^{-2} using the 1971 data (immediately following the last intensive deep and bottom water renewal) as our reference. In combination with the long-term annual average heat flux (order 70 W m^{-2}), a total flux (more than) twice as large as the long-term average is needed to bring the system back to its (1970) 1989 stage.

6. Summary and Conclusions

[56] 1. The hydrography and tracer distributions in the Greenland Sea suggest a three-layer system of the gyre: the upper mixed layer responding directly (<1 year) to the surface forcing, an intermediate layer responding to interannually variable convective activity triggered in the upper layer, and a deep and bottom layer which, during periods of weak deep convection, changes owing to admixture of water from the Arctic Ocean.

[57] 2. The vertical hydrographic and transient tracer distributions suggest that direct water mass renewal through convection did not reach deeper than 1500 m during the 1990s. Decomposing the overall density changes in the central gyre into haline and thermal contributions revealed that the GSIW became less dense through freshening and warming, while GSDW and GSBW became less dense through warming.

[58] 3. The water mass renewal was accompanied by a deepening of a subsurface temperature maximum (T_{max}) at the base of the mixed patch. Maximum T_{max} temperatures are rather constant, suggesting that no erosion (mixing) took place. To allow for sinking without erosion, the water underneath T_{max} needs to be exported laterally. The deepening of T_{max} suggests a lower limit of GSIW formation of 0.1 to 0.2 Sv and agrees with tracer data estimates [*Rhein*, 1996; *Karstensen et al.*, 2003].

[59] 4. Intensive deepening of T_{max} occurred in the first half of the 1990s when above-average heat loss, strong wind stress curl, and nearly no ice cover was observed. Possibly, the strong wind stress curl evoked a strong doming of the isopycnals in winter slumping down in summer and "pushing" T_{max} farther down in the water column. Topography at the rim of the gyre starts at about 1800 m depth and may hamper the lateral export of water and further deepening of T_{max} during the second half of the 1990s.

[60] 5. The potential vorticity of the layer underneath T_{max} revealed that the deepening initiated a restratification of the gyre that compensated for the additional shear that would be required by further deepening. The required shear is consistent with coherent vortices (CV) as the mixing agents.

[61] 6. The CV's are composed of water with high tracer content, suggesting that surface waters are participating in their formation process. In their vertical structure, they are rather similar to the gyre as a whole. In particular, they have

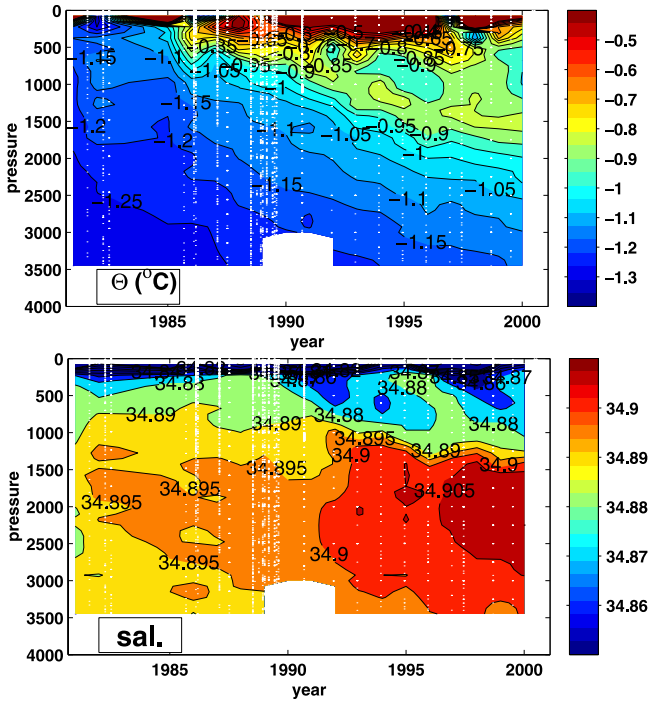

Figure 14. Temporal changes of (top) temperature and (bottom) salinity of the central Greenland Sea from 1980 to 2000. Data sources for data before 1991 are described by *Bönisch et al.* [1997].

a T_{max} structure at their base but located much deeper in the water column. This similarity may suggest similar physical processes that drive the deepening of T_{max} in the gyre and in the CVs. It further excludes an origin of T_{max} as being advected from the gyre rim.

[62] 7. Greenland Sea Intermediate Water (GSIW) changed to a warmer and less saline mode during the 1990s compared to the 1980s (Figure 14). The freshening is very likely of Arctic Ocean origin and the occurrence at the beginning of the 1990s does coincide with a strong decrease in Arctic sea ice volume [*Köberle and Gerdes*, 2003].

[63] 8. Salinity increased in the deep waters (Figure 14), particularly through the merging of the salinity gradient, associated with T_{max} and the salinity maximum originating from the Arctic Ocean inflow into the deep basin.

[64] 9. GSDW and GSBW are products of local deep convection modified by entrainment during sinking and by lateral admixture of Arctic Ocean Water. The deep waters changed to a more saline and warmer mode starting around 1980 or before and persisting throughout the 1990s at a rate of 0.001 yr^{-1} in salinity and 0.01 K yr^{-1} in temperature.

[65] 10. Since the mid-1990s the Deep and Bottom Water CFC concentrations not only decreased but homogenized in both layers suggesting a dominance admixture from the Arctic Ocean (low CFC) and virtually no addition of water from intermediate depth (higher CFC) as found in the 1980s and early 1990s [*Visbeck and Rhein*, 2000]. The decoupling of intermediate and deep layer is associated with a stability maximum at the T_{max} depth. This is in agreement with recent density and velocity fine structure measurements [*Naveira Garabato et al.*, 2004].

[66] 11. Extrapolating the observed warming and salinification trends suggests that the properties of GSDW and GSBW will match those of the Arctic Ocean in approximately 20 years from now if we assume a two-basin system.

[67] 12. Measurements to conduct water mass formation analysis as presented here need to be carried out once a year. High horizontal and vertical resolution is desirable to measure the lateral influence of newly formed waters. However, identification of causes for the changes, as a lower salinity of the Atlantic layer, a higher freshwater import from the EGC, or the absence of local ice formation, can be derived only from measurements with high temporal and vertical resolution in the upper 500 m. Further conclusions will be possible as complete seasonal cycles recorded by means of ARGO float data in the Greenland Sea gyre become available.

[68] **Acknowledgments.** The data presented here were sampled and prepared by numerous colleagues. We particularly would like to thank the captain and the crew of RV *Johann Hjort* and G. Bönisch, C. Neill, and F. Menzia. Comments from D. Quadfasel, R. Käse, and two anonymous reviewers significantly improved the manuscript. The NCEP/NCAR reanalysis data are available from the NOAA/CIRES Climate Diagnostics Center, Boulder, Colorado, USA, from their web site http://www.cdc.noaa.gov. Financial support from NOAA's Office of Global Programs and NOAA's Atlantic Climate Change Program, through grant NA86GP0375, and support through NSF fund OCE 01-18707 is acknowledged. This is LDEO contribution 6671.

References

Aagaard, K., and E. C. Carmack (1989), The role of sea ice and other fresh water in the Arctic circulation, *J. Geophys. Res.*, *94*(C10), 14,485–14,498.

Aagaard, K., J. H. Swift, and E. C. Carmack (1985), Thermohaline circulation in the Arctic Mediterranean Seas, *J. Geophys. Res.*, *90*(C3), 4833–4846.

Aagaard, K., E. Fahrbach, J. Meincke, and J. H. Swift (1991), Saline outflow from the Arctic Ocean: Its contribution to the deep waters of the Greenland, Norwegian, and Island seas, *J. Geophys. Res.*, *96*(C11), 20,433–20,441.

Akima, H. (1970), A new method of interpolation and smooth curve fitting based on local procedures, *J. Assoc. Comput. Mach.*, *17*(4), 589–602.

Alekseev, G. V., V. V. Ivanov, and A. A. Korablev (1994), Interannual variability of the thermohaline structure in the convective gyre of the Greenland Sea, in *The Polar Oceans and Their Role in Shaping the Global Environment*, *Geophys. Monogr. Ser.*, vol. 85, edited by O. M. Johannessen, R. D. Munch, and J. E. Overland, pp. 485–496, AGU, Washington, D. C.

Anderson, L. G., E. P. Jones, and B. Rudels (1999), Ventilation of the Arctic Ocean estimated by a plume entrainment model constrained by CFCs, *J. Geophys. Res.*, *104*(C6), 13,423–13,429.

Bacon, S. (1997), Decadal variability in the outflow from the Nordic Seas to the deep North Atlantic, *Nature*, *394*, 871–874.

Blindheim, J. (1990), Arctic Intermediate Water in the Norwegian Sea, *Deep Sea Res.*, *37*(9), 1475–1489.

Blindheim, J., and F. Rey (2004), Water mass formation and distribution in the Nordic Seas during the 1990s, *ICES J. Mar. Sci.*, *61*, 846–863.

Bönisch, G., and P. Schlosser (1995), Deep water formation and exchange rates in the Greenland/Norwegian Seas and the Eurasian basin of the Arctic Ocean derived from tracer balances, *Prog. Oceanogr.*, *35*, 29–52.

Bönisch, G., J. Blindheim, J. L. Bullister, P. Schlosser, and D. W. R. Wallace (1997), Long-term trends of temperature, salinity, density and transient tracers in the Greenland Sea, *J. Geophys. Res.*, *102*(C8), 18,553–18,571.

Broecker, W. S., T.-H. Peng, J. Jouzel, and G. Russell (1990), The magnitude of global fresh-water transports of importance to ocean circulation, *Clim. Dyn.*, *4*, 73–79.

Budeus, G., W. Schneider, and G. Krause (1998), Winter convective events and bottom water warming in the Greenland Sea, *J. Geophys. Res.*, *103*(C9), 18,513–18,527.

Bullister, J., and R. F. Weiss (1988), Determination of CCl_3F and CCl_2F_2 in seawater and air, *Deep Sea Res.*, *35*(5), 839–853.

Gascard, J.-C., A. J. Watson, M.-J. Messias, K. A. Olsson, T. Johannessen, and K. Simonsen (2002), Long-lived vortices as a mode of deep ventilation in the Greenland Sea, *Nature*, *416*, 525–527.

GSP group (1990), Greenland sea project, *Eos Trans. AGU*, *71*(24), 750, 751, 754, 755.
Hansen, B., and S. Osterhus (2000), North Atlantic–Nordic Seas exchange, *Prog. Oceanogr.*, *45*, 109–208.
Hansen, B., W. R. Turrell, and S. Osterhus (2001), Decreasing overflow from the Nordic Seas into the Atlantic Ocean through Faroe-Shetland Channel since 1950, *Nature*, *411*, 927–930.
Heinze, C., P. Schlosser, K. P. Koltermann, and J. Meincke (1990), A tracer study of deep water renewal in the European polar seas, *Deep Sea Res.*, *37*(9), 1425–1453.
Jakobsen, P. K., M. H. Ribergaard, D. R. Quadfasel, and T. Schmith (2003), The near-surface circulation in the northern North Atlantic as inferred from Lagrangian drifters: Variability from the mesoscale to interannual, *J. Geophys. Res.*, *108*(C8), 3251, doi:10.1029/2002JC001554.
Jakobsson, M. (2002), Hypsometry and volume of the Arctic Ocean and its constituent seas, *Geochem. Geophys. Geosyst.*, *3*(5), 1028, doi:10.1029/2001GC000302.
Jonsson, S., and H. Valdimarsson (2004), A new path for the Denmark Strait overflow water from the Iceland Sea to Denmark Strait, *Geophys. Res. Lett.*, *31*, L03305, doi:10.1029/2003GL019214.
Karstensen, J., P. Schlosser, J. Blindheim, J. Bullister, and D. Wallace (2003), On the formation of intermediate water in the Greenland Sea during the 1990s, *ICES J. Mar. Sci.*, *219*, 375–377.
Keffer, T. (1985), The ventilation of the world's oceans: Maps of the potential vorticity field, *J. Phys. Oceanogr.*, *15*, 509–523.
Köberle, C., and R. Gerdes (2003), Mechanisms determining variability of Arctic ice conditions and export, *J. Clim.*, *16*, 2843–2858.
Kwok, R., and D. A. Rothrock (1999), Variability of Fram Strait ice flux and North Atlantic oscillation, *J. Geophys. Res.*, *104*(C3), 5177–5189.
Ludin, A., R. Weppernig, G. Bnisch, and P. Schlosser (1998), Mass spectrometric measurement of helium isotopes and tritium in water samples, *Tech. Rep. 98-6*, Lamont-Doherty Earth Obs., Palisades, NY.
Marshall, J., and F. Schott (1999), Open-ocean convection: Observations, theory, and models, *Rev. Geophys.*, *37*, 1–64.
Mauritzen, C. (1996), Production of dense overflow waters feeding the North Atlantic across the Greenland-Scotland Ridge: Part 1. Evidence for a revised circulation scheme, *Deep Sea Res.*, *43*(6), 769–806.
McDougall, T. J. (1983), Greenland Sea bottom water formation: A balance between advection and double-diffusion, *Deep Sea Res., Part A*, *30*(11), 1109–1117.
McDougall, T. (1987), Neutral surfaces, *J. Phys. Oceanogr.*, *17*, 1950–1964.
Meincke, J., B. Rudels, and H. J. Friedrich (1997), The Arctic Ocean–Nordic seas thermohaline system, *ICES J. Mar. Sci.*, *54*, 283–299.
Naveira Garabato, A. C., K. I. C. Oliver, A. J. Watson, and M.-J. Messias (2004), Turbulent diapycnal mixing in the Nordic seas, *J. Geophys. Res.*, *109*, C12010, doi:10.1029/2004JC002411.
Osterhus, S., and T. Gammelsrod (1999), The abyss of the Nordic Seas is warming, *J. Clim.*, *12*, 3297–3304.
Pond, S., and G. L. Pickard (1983), *Introductory Dynamical Oceanography*, 329 pp., Elsevier, New York.
Poulain, P.-M., A. Warn-Varnas, and P. P. Niiler (1996), Near-surface circulation of the Nordic seas as measured by Lagrangian drifters, *J. Geophys. Res.*, *101*(C8), 18,237–18,258.
Prinn, R. G., et al. (2000), A history of chemically and radiatively important gases in air deduced from ALE/GAGE/AGAGE, *J. Geophys. Res.*, *105*(D14), 17,751–17,792.
Rahmstorf, S. (1994), Rapid climate transitions in a coupled ocean-atmosphere model, *Nature*, *372*, 82–85.
Renfrew, I. A., G. W. K. Moore, P. S. Guest, and K. Bumke (2002), A comparison of surface-layer and surface turbulent-flux observations over the Labrador Sea with ECMWF analyses and NCEP reanalyses, *J. Phys. Oceanogr.*, *32*, 383–400.
Rhein, M. (1996), Convection in the Greenland Sea, 1982–1993, *J. Geophys. Res.*, *101*(C8), 18,183–18,192.
Roemmich, D. (1983), Optimal estimation of hydrographic station data and derived fields, *J. Phys. Oceanogr.*, *13*, 1544–1549.
Roether, W., B. Klein, and K. Bulsiewics (2001), Apparent loss of CFC-113 in the upper ocean, *J. Geophys. Res.*, *106*(C2), 2679–2688.
Rudels, B. (1990), Haline convection in the Greenland Sea, *Deep Sea Res.*, *37*(9), 1491–1511.
Rudels, B., D. Quadfasel, H. Friedrich, and M.-N. Houssais (1989), Greenland Sea convection in the winter of 1987–1988, *J. Geophys. Res.*, *94*(C3), 3223–3227.
Rudels, B., R. Meyer, E. Fahrbach, V. Ivanov, S. Osterhus, D. Quadfasel, U. Schauer, V. Tverburg, and R. A. Woodgate (2000), The water mass distribution in Fram Strait and over the Yermak Plateau in summer 1997, *Ann. Geophys.*, *18*, 687–705.
Schlosser, P., G. Bönisch, M. Rhein, and R. Bayer (1991), Reduction of deep water formation in the Greenland Sea during the 1980s: Evidence from tracer data, *Science*, *251*, 1054–1056.
Send, U., and J. Marshall (1995), Integrals effect of deep convection, *J. Phys. Oceanogr.*, *25*, 855–872.
Smethie, W. M., H. G. Ostlund, and H. H. Loosli (1986), Ventilation of the Greenland and Norwegian Sea: Evidence from krypton-85, tritium, carbon-14 and argon-39, *Deep Sea Res.*, *33*(5), 675–703.
Smith, S. R., D. M. Legler, and K. V. Verzone (2001), Quantifying uncertainties in NCEP reanalysis using high-quality research vessel observations, *J. Clim.*, *14*, 4062–4072.
Swift, J. H., and K. Aagaard (1981), Seasonal transitions and water mass formation in the Iceland and Greenland Sea, *Deep Sea Res., Part A*, *28*(10), 1107–1129.
Swift, J. H., and K. P. Koltermann (1988), The origin of Norwegian Sea deep-waters, *J. Geophys. Res.*, *93*(C9), 3563–3569.
Swift, J. H., K. Aagaard, and S. Malmberg (1980), The contribution of the Denmark Strait overflow to the deep North Atlantic, *Deep Sea Res., Part A*, *27*(1), 29–42.
Toudal, L. (1999), Ice extent in the Greenland Sea 1978–1995, *Deep Sea Res., Part II*, *46*(6-7), 1237–1254.
Vellinga, M., and R. A. Wood (2002), Global climatic impacts of a collapse of the Atlantic thermohaline circulation, *Clim. Change*, *54*, 251–267.
Visbeck, M., and M. Rhein (2000), Is bottom boundary layer mixing slowly ventilating Greenland Sea deep water?, *J. Phys. Oceanogr.*, *30*, 215–224.
Wadhams, P., J. Holfort, E. Hansen, and J. P. Wilkinson (2002), A deep convective chimney in the winter Greenland Sea, *Geophys. Res. Lett.*, *29*(10), 1434, doi:10.1029/2001GL014306.
Walker, S. J., R. F. Weiss, and P. K. Salameh (2000), Reconstructed histories of the annual mean atmospheric mole fractions for the halocarbons CFC-11, CFC-12, CFC-113 and carbon tetrachloride, *J. Geophys. Res.*, *105*(C6), 14,285–14,296.
Wilkinson, J. P., and P. Wadhams (2003), A salt flux model for salinity change through ice production in the Greenland Sea and its relationship to winter convection, *J. Geophys. Res.*, *108*(C5), 3147, doi:10.1029/2001JC001099.

J. Blindheim, Havforskningsinstituttet, Postboks 1870 Nordnes, N-5817 Bergen, Norway. (john.blindheim@imr.no)
J. L. Bullister, NOAA/Pacific Marine Environmental Laboratory, R/E/PM, Bin C15700, Pacific Marine Environmental Laboratory, NOAA Building 3, 7600 Sand Point Way NE, Seattle, WA 98115-0007, USA. (john.l.bullister@noaa.gov)
J. Karstensen and D. W. R. Wallace, Leibniz Institut für Meereswissenschaften an der Universität Kiel (IFM-GEOMAR), Düsternbrooker Weg 20, D-24105 Kiel, Germany. (jkarstensen@ifm-geomar.de; dwallace@ifm-geomar.de)
P. Schlosser, Lamont-Doherty Earth Observatory of Columbia University, P.O. Box 1000, 61 Route 9W, Palisades, NY 10964-1000, USA. (schlosser@ldeo.columbia.edu)